Arch Computat Methods Eng (2018) 25:165–193
https://doi.org/10.1007/s11831-017-9233-4

S.I.: MACHINE LEARNING IN COMPUTATIONAL MECHANICS

WYPiWYG Damage Mechanics for Soft Materials: A Data-Driven Approach

Mar Miñano[1] · **Francisco J. Montáns**[1]

Received: 13 April 2017 / Accepted: 24 May 2017 / Published online: 12 June 2017

Abstract The conservative elastic behavior of soft materials is characterized by a stored energy function which shape is usually specified a priori, except for some material parameters. There are hundreds of proposed stored energies in the literature for different materials. The stored energy function may change under loading due to damage effects, but it may be considered constant during unloading–reloading. The two dominant approaches in the literature to model this damage effect are based either on the Continuum Damage Mechanics framework or on the Pseudoelasticity framework. In both cases, additional assumed evolution functions, with their associated material parameters, are proposed. These proposals are semi-inverse, semi-analytical, model-driven and data-adjusted ones. We propose an alternative which may be considered a non-inverse, numerical, model-free, data-driven, approach. We call this approach WYPiWYG constitutive modeling. We do not assume global functions nor material parameters, but just solve numerically the differential equations of a set of tests that completely define the behavior of the solid under the given assumptions. In this work we extend the approach to model isotropic and anisotropic damage in soft materials. We obtain numerically the damage evolution from experimental tests. The theory can be used for both hard and soft materials, and the infinitesimal formulation is naturally recovered for infinitesimal strains. In fact, we motivate the formulation in a one-dimensional infinitesimal framework and we show that the concepts are immediately applicable to soft materials.

✉ Francisco J. Montáns
fco.montans@upm.es

Mar Miñano
mar.mnunez@upm.es

[1] Escuela Técnica Superior de Ingeniera Aeronáutica y del Espacio, Universidad Politécnica de Madrid, Pza.Cardenal Cisneros, 28040 Madrid, Spain

1 Introduction

The basic ingredient to model the behavior of soft materials like rubber [1–3] or biological tissues [4–6] is hyperelasticity. Hyperelastic behavior constitutes the basic non-dissipative elastic behavior at large strains [2] and as so, it is equivalent to the elastic behavior at small strains. However, whereas path independence is fulfilled at small strains by the symmetry of the elasticity tensor, at large strains some integrability requirements need to be fulfilled. Nowadays the simplest and standard way to do so is to assume an *analytical* strain energy density function from which the stresses are obtained as a function of the strains. Some material parameters permit the different assumed stored energies to fit available experimental data, and because of the variable success of these energies when addressing different materials, there are hundreds of strain energy proposals in the literature. For isotropic materials the Neo-Hookean model [7] is the simplest one, and the Ogden model [8] one of the most successful ones. For anisotropic materials there are mainly two approaches. The first one is purely phenomenological. The models of Fung [9] and Itskov and Ehret [11, 10] for biological tissues and Itskov and Aksel [12] for rubber-like materials, are some examples. The other approach is structure-based, inherited from the mechanics of composite materials [15]. The models of Lanir [13], Humphrey and Yin [14], Holzapfel et al. [15], and Gasser et al. [16] are examples of this kind. In all these models, it is frequent to use optimization algorithms to obtain the material parameters [17–19]. Non-uniqueness of

these parameters is a well known and frequently reported problem. These models may also lack numerical material-symmetries congruency [20]. Furthermore, in the case of structure-based models, it is necessary to properly account for fibers working in tension and (not) working in compression [21], they may present unrealistic transverse strains [22, 23] and are frequently fitted with incomplete material data resulting in arbitrary behavior in other loading situations [24]. Many of these models are not compatible with the full infinitesimal theory for their respective symmetry groups [25, 26].

Rubber-like materials and biological tissues exhibit a softening phenomenon known as Mullins effect [27, 28]. In the case of carbon-filled rubber materials it is attributed to bond rupture between polymeric chains [29, 30], slipping [31], disentanglement [32], filler rupture [33] and between them and the filler [34, 35]. A review for rubber-like solids is given by Diani et al. [35]. For the case of biological tissues, it is attributed to the permanent orientation of collagen fibres and breakage of collagen fibrils [38, 39] and of proteoglycans [36, 37, 40]. Whereas in hard materials there are many possible approaches to model damage in general (see review in [41]), in soft materials fewer approaches have been followed.

The most used formulation for soft materials is the Continuum Damage Mechanics (CDM) approach. In this approach, a hypothetical undamaged energy is penalized by a damage coefficient $(1-D)$, where $D \in (0,1]$ is the damage variable of Rabotnov. For isotropic materials the formulation of Simo [42] is one of the best known references, see also [43, 44]. This framework has been extended to anisotropic materials employing different strain energy functions and different damage evolution equations. For example in Calvo et al. [45], different damage parameters D_m and D_f for matrix and fibers are considered and associated exponential-type expressions are employed in terms of Simo energy strains. The same group has extended the model to capture permanent set [46], viscous effects [47] and additional continuous damage [48]. A comparison of damage functions in soft tissue can be found in Peña [47] and in Balzani and Schmidt [50]. A comparison of continuous and discontinuous damage functions can be found in [48], where they conclude that continuous damage may be used only to model hysteresis and stabilization in the first cycles of the loading path because of the rapid damage saturation. Damage has also been used to characterize the irreversible stress drop in rectus sheath [51]. Localization of damage (and hence mesh dependency) may happen in these cases [49] as it is well known [52], but the quasi-incompressible nature of soft tissues helps to regularize the problem [53]. In this last work, a mixture theory is employed to account for non-affine deformations and they capture the monotonic loading experiments of Martins et al. [51]. This framework has also been used by Sáez et al. [54] to develop a microsphere-based approach to damage in soft fibred tissue. The microsphere approach had been previously used by Miehe et al. [55–57] for elastomers and by Caner and Carol [58] and Alastrué et al. [59] for biological tissues. The continuum damage formulation has also been extended to include smooth muscle cells in arteries [60]. Active damage has also been included in the different damage formulation in [10], which includes damage from evolution functions of the structural tensors in order to guarantee polyconvexity. Polyconvex energy functions with damage have also been used in [61]. Similar conceptual formulations by direct modification of the energy function and more oriented to failure are found in the works of Volokh [62, 63]. Other formulations including a damage evolution function in terms of the fourth Spencer invariant may be found in [64]. The continuum damage framework has also been employed at different scales. In [89] a microstructural damage for fibers which links damage with fiber recruiting distribution is formulated and the result compared with CDM and Pseudoelasticity. In Schmidt et al. [65] statistical distributions of quantities at the collagen fibril level, including the proteoglycans orientation are introduced in order to enhance the microstructural understanding of the behavior of the tissue. With the same purpose Blanco et al. [66] have developed a model at the mesoscale in which inelastic phenomena in the fibre is assumed to be caused only by degradation processes in the fibrils by means of two failure modes. In a more general setting, truss-like microstructures with damage following the same framework have been formulated via relaxed incremental variational formulations as to avoid loss of convexity and their related problems [67]. This relaxed formulation was subsequently applied to model damage-induced hysteresis in arterial walls [68].

Another type of formulation which seems to be successful is the Pseudoelasticity framework of Ogden and Roxburgh [69]. In this framework, a pseudo-elastic potential is formulated which includes the "dissipation" due to damage and specially to cyclic loading (a feature not modelled in the discontinuous CDM framework). This approach has been followed by Dorfmann and Ogden [70] to accurately model the cyclic hysteretic behavior of a rubber compound 60phr of Carbon black after preconditioning and then extended to model the permanent set present in these materials [71] and thereafter to model changes in material symmetry in [72]. This same model was also applied to model the muscle of tobacco hornworm caterpillar *Manduca sexta*, including the active muscle effect [73] and also in [48] to simulate anisotropic damage in fibrous biological tissues. The thermodynamics of Pseudoelasticity is studied in [74], where they argue that the usual pseudoelastic materials do not dissipate the energy (for example into heat) but store it. Hence a modification is therein proposed. On

the other hand, a practical comparison between pseudo-elastic and continuum damage models for modelling Mullins effect can be found in Gracia et al. [75]. Here we note that both CDM and Pseudoelasticity are built on the idea of the existence of a hypothetical undamaged energy. From a practical point of view, since the material parameters of these models are typically obtained through optimization algorithms like the Levenberg–Marquardt algorithm [76] or by sensitivity analysis, its physical meaning has no actual relevance. However, it is apparent that the undamaged energy does not exist because any loading from virgin state entails itself a damage process, i.e. the primary loading curve does not proceed from a hyperelastic behavior. Then, that hypothetical undamaged energy which is the conceptual basis of both CDM and Pseudoelastic formulations, cannot be measured neither directly, nor indirectly through stress–strain curves.

Let us summarize the ideas behind the commented approaches in few words. Hyperelasticity is modelled through *assumed* analytical stored energy function shapes. These shapes are *best-fitted* to experimental data through some additional material parameters. Damage is modelled through different formulations which again *assume* the shape of some undamaged stored energy functions and also *assume* an evolution equation. This evolution equation is also *best-fitted* to experimental data through some material parameters. Conceptually, this is a semi-inverse global approach similar to the global approach followed by Rayleigh to compute natural frequencies and deflections in plates: a global analytical solution is assumed except for some global parameters that are computed as to obtain a best fit of the corresponding energy of the structure. This global approach has been superseded in practice by the local interpolating approach given, for example by finite elements.

In the last years we have been pursuing the different, local approach. The idea behind the approach is to avoid the use of analytical stored energy functions (with all the mentioned problems) but instead to obtain the stored energy directly from experimental data using a numerical procedure and local interpolations. We have named it the "What-You-Prescribe-Is-What-You-Get" (WYPiWYG) approach [77] because as the name claims, the modeler may get from simulations "exactly" (i.e. to the desired precision) the prescribed data, and the prescribed data is a complete set of experimental tests; for example six curves (including the compression part when applicable) for incompressible orthotropic materials. The models are based on a spline (local) interpolation between terms of the derivative of the stored energy which are obtained numerically solving the equilibrium equations of the tests. The first model of this kind is that of Sussman and Bathe [78] for incompressible isotropic materials which use the Kaersley and Zapas formula. We have developed WYPiWYG formulations for transversely isotropic [79], orthotropic [77] and isotropic compressible materials [80]. A general procedure without inversion formula is given in ref. [81]. For example WYPiWYG formulations, which are a natural extension of the infinitesimal theory, are capable of capturing to any desired precision and in any loading situation the behavior of any isotropic compressible model following the Valanis–Landel decomposition using just the predictions from a uniaxial tension-compression test. Furthermore, the orthotropic incompressible WYPiWYG model captures exactly six experimental, independent stress–strain curves which define the material behavior in the same way that six moduli do it in the infinitesimal framework. In fact, WYPiWYG anisotropic formulations are in agreement with the corresponding infinitesimal theory at all deformation levels [25, 26] and preserve material-symmetries congruency [20]. These procedures have also been used successfully in modelling very accurately soft biological tissues [22, 81–83] and have been used also in anisotropic viscoelasticity [84, 85] to model independently equilibrated and nonequilibrated stored energies. These viscoelastic models have been also formulated mimicking the infinitesimal theory.

The purpose of this work is to extend the approach to model Mullins-type damage effects in rubber-like materials and soft biological tissues. The basic ideas are given for isotropic materials in [86]. Herein we address a motivation with comparison with similar frameworks as those of the CDM and Pseudoelasticity approaches, the finite element implementation and the extension to anisotropy. In this approach we do not make a hypothesis on any undamaged stored energy. We do not use explicit evolution equations and we do not employ material parameters nor optimization algorithms. We just employ directly stress–strain data to extract all the needed information with the minimum hypotheses. Then, the primary loading and master hyperelastic unloading–reloading curves may be captured to any desired numerical precision. The formulation may be employed also to model biological tissues because damage in the isotropic matrix and the anisotropic deviation may be modelled independently. WYPiWYG damage mechanics can be considered a model-free data-driven procedure, because no explicit analytical expression is assumed, but the behavior (i.e. "model") is learned from data.

The rest of the manuscript is structured as follows. First we motivate the concepts and theory using an infinitesimal one-dimensional example. Then we introduce the continuum theory and develop the numerical integration algorithm. Subsequently we explain how to extract the information from typical experiments. The last part of the manuscript is devoted to numerical examples under homogeneous deformations (stress-point examples) and under nonhomogeneous

ones (finite element simulations). Both isotropic and anisotropic examples are given.

2 One-Dimensional, Infinitesimal Motivation

It will be seen below that the fully nonlinear 3D formulation is obtained from an adequate one-dimensional formulation. Since concepts are easily understood in that 1D infinitesimal formulation, we address in this section this simple formulation. Thereafter, the extension to the general nonlinear case is conceptually simple.

2.1 Damage Potentials and the Multiplier Function

Consider a rheological model consisting of two springs in parallel like the ones shown in Fig. 1a. Assume for simplicity that they have the same stiffness E but different strength. As shown in Fig. 1a, when the system is stretched by a strain ε, we need a given load σ. If the stiffness of both springs is the same, each spring is loaded by equilibrium with half the stress, i.e. $\sigma/2$. The energy stored by each spring $\mathcal{W}_i\,(i=1,2)$ is

$$\mathcal{W}_i = \frac{1}{2}\sigma_i\varepsilon = \frac{1}{2}\left(\frac{\sigma}{2}\right)\varepsilon = \frac{1}{4}\sigma\varepsilon = \frac{1}{2}E\varepsilon^2 \tag{1}$$

and the energy of the system is

$$\mathcal{W} = \sum_{i=1}^{2}\mathcal{W}_i = \frac{1}{2}(2E)\varepsilon^2 = E\varepsilon^2 \tag{2}$$

When one spring reaches the maximum load and breaks apart, the energy of that spring is released, as shown in Fig. 1b, and the stiffness of the system reduces to E. If load control is imposed as shown in Fig. 1b, then after an horizontal path in the $\sigma-\varepsilon$ plot (obviously a transient dynamic effect herein not considered is present), the slope is E. However, in order to keep the stress σ in the system, an energy needs to be introduced through an increment of strain, of quantity 2ε. The energy released is

$$\mathcal{G} = \frac{1}{2}E\varepsilon^2 \tag{3}$$

and the new stored energy is

$$\mathcal{W}(2\varepsilon) = \frac{1}{2}E(2\varepsilon)^2 = 2E\varepsilon^2 \tag{4}$$

Therefore, the input energy needed to reach that stress–strain level is

$$W(\varepsilon) = \mathcal{W} + \mathcal{G} = 2E\varepsilon^2 + \frac{1}{2}E\varepsilon^2 = \frac{5}{2}E\varepsilon^2 \tag{5}$$

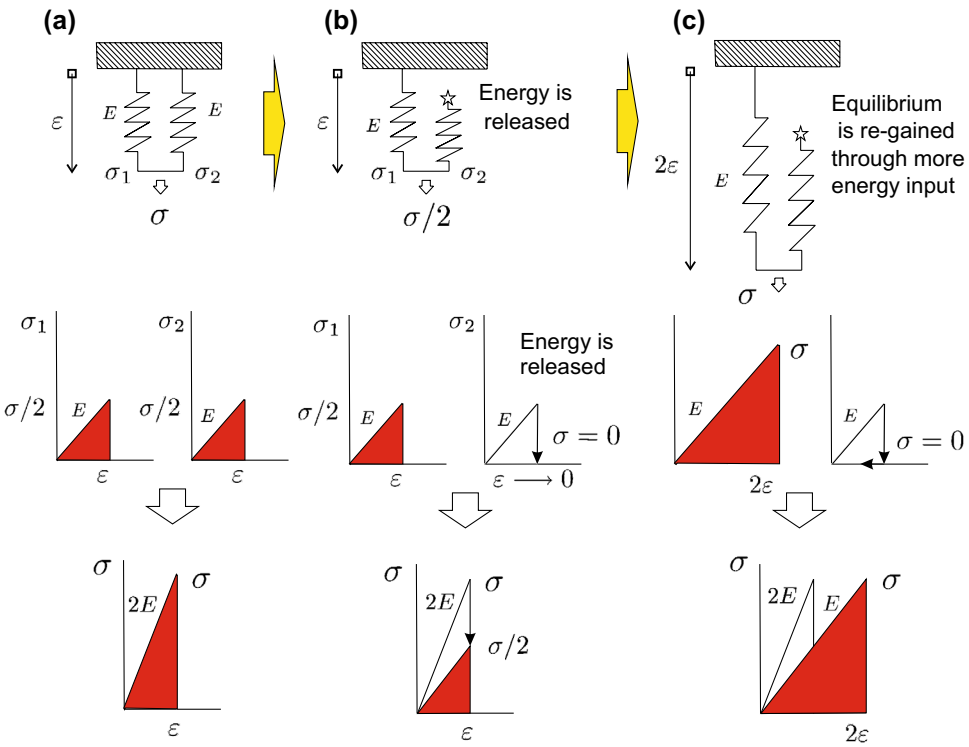

Fig. 1 Damage viewed as local fracture: 1D spring model showing energy balance

Here we note that there is a conceptual important difference between damage and plasticity. This difference is depicted in Fig. 2. Whereas in damage the energy is released, and hence has elastic nature (it is previously stored elastic energy what is being released), the energy in plasticity is incrementally dissipated. In this respect, damage is similar to fracture mechanics, being the former local, at the microscale, whereas the latter is global, at a larger scale. As a consequence, as seen in Fig. 2a, when only damage is present, there is only one possible path to reach a given stress–strain pair. On the contrary, in plasticity there are infinite possible paths to reach the same pair, see Fig. 2b. Hence an overall potential that describes the problem may be postulated. In fracture mechanics that potential is, for example, the potential energy. That is the idea behind Pseudoelasticity [69, 70]. In fact, we can consider W as a pseudoelastic energy potential similar to that proposed in [69, 70]. However, the procedure we follow herein is different from that given in those references, because, as mentioned, instead of proposing analytical functions, we address the problem numerically.

The total elastic potential energy (stored and released) W may be written as a function of the strain ε and an additional variable which determines the unloading point. Some of the first uniaxial damage models used the maximum attained strain as the damage variable, see for example [90]. However, this is not a variable useful for three-dimensional analysis. Hence, it is more frequent now to use a variable which is obtained from the maximum stored energy, see for example [42, 43, 47], among others. Nonetheless we note that during a damage process, it should be possible to model the case when damage evolves and the stored energy is decreasing; the case when all new input energy is released and that input provokes the release of already stored energy; i.e. the unstable case leading to fracture propagation. In such cases the stored energy would not be an adequate damage parameter because it is not monotonically increasing. However there are other possibilities as the energy release rate $\mathcal{G}$ or the maximum input (elastic) energy W. In the initial formulation below we choose the latter to explain concepts, although when developing the computational algorithm we will use the stored elastic energy $\mathcal{W}$ because in the cases addressed herein, it yields a simpler algorithm, and both cases are equivalent in the case $\dot{\mathcal{W}} > 0$ when $\dot{\mathcal{G}} > 0$.

We postulate the existence of the pseudoelastic energy potential $W(\varepsilon, w)$, where we define

$$w = \max_{\tau \in (-\infty, t)} W \tag{6}$$

which precludes healing, that may be a relevant aspect in soft biological tissues but which we do not model here (it would entail a healing equation for w). From this definition, the damage criterion and damage evolution condition are immediately established:

$$\begin{cases} \text{If } f = W - w < 0 \text{ then } \dot{w} = 0 \\ \text{If } f = W - w = 0 \text{ then } \dot{w} = \dot{W} \geq 0 \end{cases} \tag{7}$$

Consider a simple bi-linear case as shown in Fig. 3. The example is essentially valid either if we consider an initial

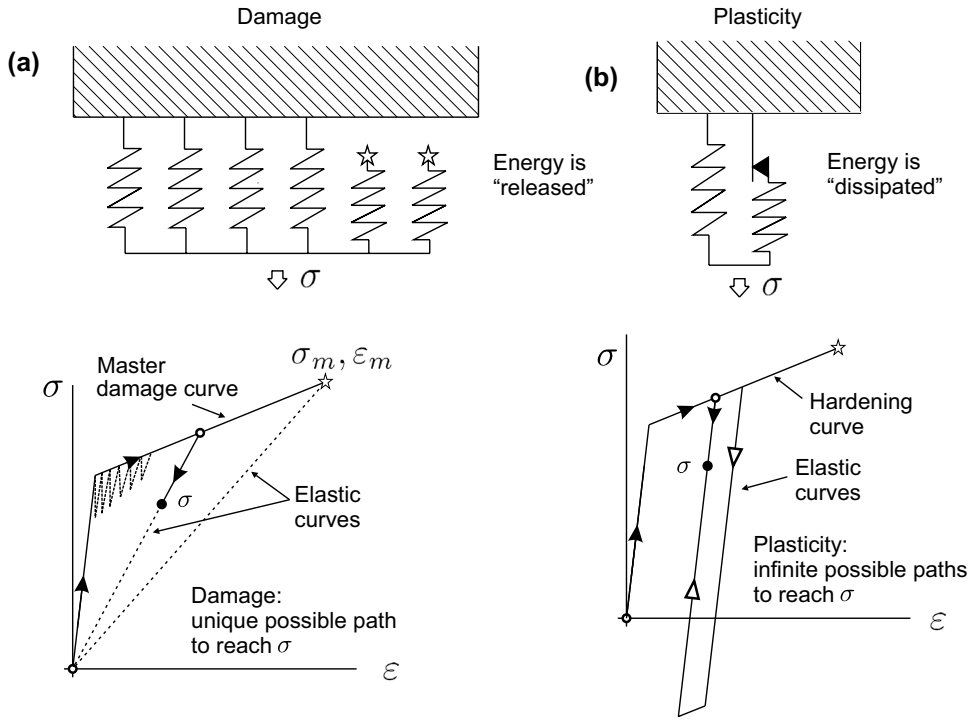

Fig. 2 Difference between damage and plasticity: path-independency in the $\sigma - \varepsilon$ space

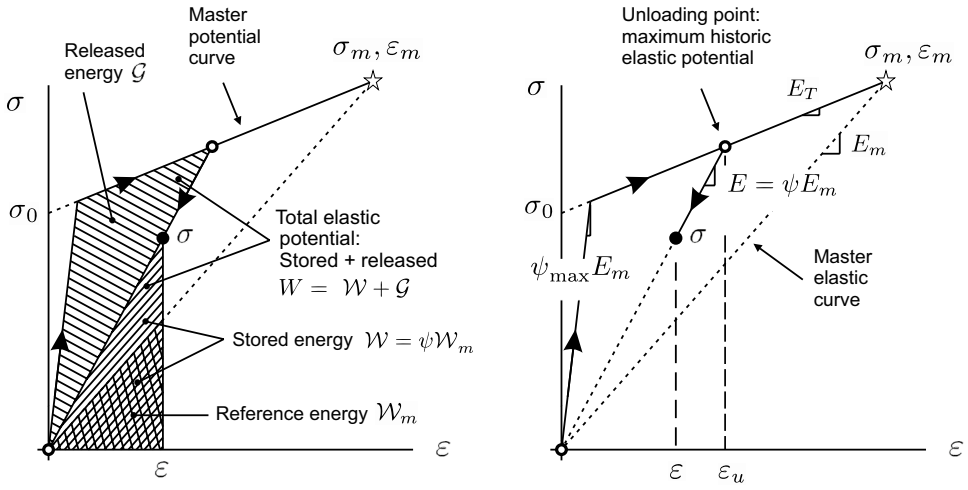

Fig. 3 The bilinear model. *Left* released elastic energy $\mathcal{G}$, elastic stored energy $\mathcal{W}$, reference elastic energy $\mathcal{W}_m$ and total elastic potential W. *Right* reference elastic modulus E_m, current elastic modulus $E = \psi E_m$ and tangent modulus during primary loading E_T

undamaged domain characterized by a maximum Young modulus E_0 or the absence of that domain, where damage begins at a stress value of σ_0. In Fig. 3 we show the stored energy $\mathcal{W}$, the released energy $\mathcal{G}$ and the total elastic energy (stored plus released) $W = \mathcal{W} + \mathcal{G}$. Assume that the maximum stress–strain admissible in the material is given by $(\varepsilon_m, \sigma_m)$; alternatively one may consider these values just as the reference ones. Without loss of generality, assume also that the initial elastic slope is rigid, $E_0 \to \infty$. In the right plot of Fig. 3 we show some immediate relations using the multiplier function within the domain $\psi \in [0, \infty)$ (although we will assume herein $\psi \geq 1$). The elastic moduli may be related through a scalar function such that

$$E = \psi E_m \tag{8}$$

If $\psi = 1$ we obtain the reference modulus E_m—here m stands for master. At a given unloading point characterized by the unloading strain ε_u we can write

$$\begin{aligned} \mathcal{W}(\varepsilon_u, \psi(w)) &= \tfrac{1}{2} E \varepsilon_u^2 \\ &= \tfrac{1}{2} \psi(w) E_m \varepsilon_u^2 = \psi(w) \mathcal{W}_m(\varepsilon_u) \end{aligned} \tag{9}$$

where $\mathcal{W}_m(\varepsilon_u)$ is the reference energy for the strain ε_u, which is independent of ψ. During unloading–reloading, ψ remains constant and

$$\mathcal{W}(\varepsilon_u, \psi = const) = \tfrac{1}{2} \psi E_m \varepsilon^2 \tag{10}$$

and

$$\sigma = \left. \frac{\partial \mathcal{W}}{\partial \varepsilon} \right|_{\psi = const} = \psi E_m \varepsilon =: \psi \sigma_m(\varepsilon) \tag{11}$$

where $\sigma_m(\varepsilon)$ is the master elastic curve; i.e. that for $\psi = 1$ with a stored energy $\mathcal{W}_m(\varepsilon)$. Consider now the unloading stress σ_u given by the virgin (primary, pseudoleastic) loading curve

$$W(\varepsilon) = \sigma_0 \varepsilon + \frac{1}{2} E_T \varepsilon^2 \tag{12}$$

so we write $\sigma_u = dW(\varepsilon_u)/d\varepsilon_u$. Note that the case in which $E_0 \nrightarrow \infty$, may be given by

$$W(\varepsilon) = \sigma_0 \varepsilon + \frac{1}{2} E_T \varepsilon^2 - \frac{1}{2} \sigma_0 \varepsilon_0 \tag{13}$$

where $\varepsilon_0 \approx \sigma_0 / E_0$ is the maximum strain without damage. The consistency condition at the onset of unloading requires

$$\sigma_u = \frac{dW(\varepsilon_u)}{d\varepsilon_u} = \left. \frac{\partial \mathcal{W}(\varepsilon, \psi)}{\partial \varepsilon} \right|_{\substack{\varepsilon = \varepsilon_u \\ \psi = const}} = \psi \sigma_m(\varepsilon_u) \tag{14}$$

so we can immediately obtain

$$\psi(\varepsilon_u) = \frac{E(\varepsilon_u)}{E_m} = \frac{\sigma_u(\varepsilon_u)}{\sigma_m(\varepsilon_u)} \equiv \frac{dW/d\varepsilon_u}{d\mathcal{W}_m/d\varepsilon_u} = \frac{\mathcal{W}(\varepsilon_u)}{\mathcal{W}_m(\varepsilon_u)} \tag{15}$$

i.e. the $\psi(\varepsilon_u)$ function is obtained as the ratio between the primary loading curve and the master elastic curve. For the bi-linear case at hand

$$\psi(\varepsilon_u) = \frac{\sigma_0 + E_T \varepsilon_u}{E_m \varepsilon_u} \tag{16}$$

and using Eqs. (12) and (6)

$$\begin{cases} \psi(w) = \dfrac{E_T}{E_m} \dfrac{\sqrt{\sigma_0^2 + 2E_T w}}{\sqrt{\sigma_0^2 + 2E_T w} - \sigma_0} \text{ for } E_T \neq 0 \\ \psi(w) = \dfrac{\sigma_0^2}{E_m w} \text{ for } E_T = 0 \end{cases} \tag{17}$$

Alternatively, assuming that $\mathcal{W}(\varepsilon, \psi)$ is a monotonically increasing function of ε, there is a one-to-one relation between $\mathcal{W}_m(\varepsilon_u)$ and $W(\varepsilon_u)$, and also between $\mathcal{W}(\varepsilon_u)$ and $W(\varepsilon_u)$, so we can express ψ in other alternative forms. Defining $w_D := \mathcal{W}(\varepsilon_u)$ and using

$$\varepsilon_u = \sqrt{\frac{2\mathcal{W}(\varepsilon_u)}{E}} = \sqrt{\frac{2\mathcal{W}(\varepsilon_u)}{\psi E_m}} \tag{18}$$

after a little algebra we obtain

$$\psi(w_D) = \frac{1}{8E_m w_D}\left(\sigma_0 + \sqrt{\sigma_0^2 + 8E_T w_D}\right)^2 \tag{19}$$

with the obvious limit $\psi \longrightarrow \infty$ when $\mathcal{W} = 0$. Of course these equations may be inverted to give for example

$$w_D(\psi) = \frac{\psi\sigma_0^2 E_m}{2\psi^2 E_m^2 + 2E_T^2 - 4\psi E_T E_m} \tag{20}$$

and for the case $E_T \neq 0$ (the other one is trivial)

$$w(\psi) = \frac{2\psi\sigma_0^2 E_m - \sigma_0^2 E_T}{2\psi E_m^2 + 2E_T^2 - 4\psi E_T E_m} \tag{21}$$

We note that even though in the general nonlinear case these functions $\psi(w)$, $\psi(w_D)$, $w(\psi)$, $w_D(\psi)$ may not be explicitly computed in closed form, they can be generated using piecewise cubic splines from the same curves. The inverse operations in this context is also simply; one just need to sample the original function and build the spline with the axes interchanged. We remark that Eq. (15) is essentially uniaxial, and valid in 1D, but Eq. (19) is valid in the general 3D case.

2.2 One-Dimensional Infinitesimal Framework in Terms of the Pseudoelastic Potential W

This framework may be conceptually closer to the Ogden and Roxburgh Pseudoelastic theory. Once the previous functions have been computed, the continuum damage theory is simple. The stress power is

$$\mathcal{P} = \sigma\dot{\varepsilon} = \dot{W} = \frac{dW}{d\varepsilon}\dot{\varepsilon} \tag{22}$$

where the stresses are the total derivative of the total (pseudo-)elastic potential W which characterizes the (pseudoelastic) primary loading i.e. $\sigma = dW/d\varepsilon$. The rate is

$$\begin{aligned}\dot{W}(\varepsilon, w(\varepsilon)) &= \left.\frac{\partial W(\varepsilon, w)}{\partial \varepsilon}\right|_{\dot{w}=0}\dot{\varepsilon} + \left.\frac{\partial W(\varepsilon, w)}{\partial w}\right|_{\dot{\varepsilon}=0}\dot{w} \\ &= \underbrace{\left.\frac{\partial W(\varepsilon, w)}{\partial \varepsilon}\right|_{\dot{w}=0}\dot{\varepsilon}}_{\text{predictor ("trial")}} + \underbrace{\left.\frac{\partial W(\varepsilon, w)}{\partial w}\right|_{\dot{\varepsilon}=0}\frac{dw}{d\varepsilon}\dot{\varepsilon}}_{\text{corrector}}\end{aligned} \tag{23}$$

$$\dot{W}(\varepsilon, w(\varepsilon)) = {}^{tr}\dot{W} + {}^{ct}\dot{W} \tag{24}$$

$$\dot{W}(\varepsilon, w(\varepsilon)) = {}^{tr}\sigma\dot{\varepsilon} + {}^{ct}\sigma\dot{\varepsilon} = \sigma\dot{\varepsilon} \tag{25}$$

The first term ${}^{tr}\sigma$ is the predictor term (which can also be named the undamaged stress), whereas the last one is the corrector one (damage stress reduction) see Fig. 1a, b. The stress is decomposed as

$$\sigma = {}^{tr}\sigma + {}^{ct}\sigma = {}^{tr}\sigma - L \tag{26}$$

The predictor term is the partial derivative when the energy release is frozen, i.e. all the input energy is accepted as elastic and will be either stored in $\mathcal{W}$ or released

$${}^{tr}\sigma = \left.\frac{\partial W(\varepsilon, w)}{\partial \varepsilon}\right|_{\dot{w}=0} \tag{27}$$

We call the second term

$$L = \frac{d\mathcal{L}}{d\varepsilon} = -\left.\frac{\partial W(\varepsilon, w)}{\partial w}\right|_{\dot{\varepsilon}=0}\frac{dw}{d\varepsilon} = -{}^{ct}\sigma > 0 \tag{28}$$

the *lost energy rate*, i.e. $\mathcal{L}$ is the energy which never enters the system because of damage evolution; it is not equal to the released energy $\mathcal{G}$, because the former has never been stored. We can write

$$L = \lambda\frac{dw}{d\varepsilon} \text{ where } \lambda = -\left.\frac{\partial W(\varepsilon, w)}{\partial w}\right|_{\dot{\varepsilon}=0} \geq 0 \tag{29}$$

as the *energy loss factor*. During unloading–reloading damage evolution vanishes, so $\dot{w} = 0$ and the lost energy rate L vanishes. Hence noting that we can invert the function $w(\psi)$ to obtain $\psi(w)$ or $\psi\left(w_D\right)$, we get

$$\frac{dW}{d\varepsilon} = \left.\frac{\partial W(\varepsilon, w(\psi))}{\partial \varepsilon}\right|_{\dot{w}=0} \tag{30}$$

$$= \left.\frac{\partial \mathcal{W}(\varepsilon, \psi(w_D))}{\partial \varepsilon}\right|_{\dot{\psi}=0} = \frac{\partial \mathcal{W}}{\partial \varepsilon} = \sigma \tag{31}$$

when $\dot{w} = 0$. Because during damage evolution, by definition of w

$$f := W - w = 0 \text{ and } \dot{f} = \dot{W} - \dot{w} = 0 \tag{32}$$

and hence $dW/d\varepsilon = dw/d\varepsilon$, we obtain from Eq. (23)

$$\sigma = \psi \frac{d\mathcal{W}_m}{d\varepsilon} \equiv \frac{dW(\varepsilon, w)}{d\varepsilon} = \frac{1}{1+\lambda} \frac{\partial \mathcal{W}(\varepsilon, w)}{\partial \varepsilon} = \frac{1}{1+\lambda}\, {}^{tr}\sigma \tag{33}$$

The continuum tangent modulus during damage evolution is obtained as

$$E_T = \frac{d^2 W(\varepsilon, w)}{\partial \varepsilon^2} = \frac{d}{d\varepsilon}\left(\psi \frac{d\mathcal{W}_m}{d\varepsilon}\right) \tag{34}$$

$$E_T = \frac{d^2 W(\varepsilon, w)}{\partial \varepsilon^2} = \psi \frac{d^2 \mathcal{W}_m}{d\varepsilon^2} + \frac{d\psi}{d\varepsilon}\sigma_m \tag{35}$$

$$E_T = \frac{d^2 W(\varepsilon, w)}{\partial \varepsilon^2} = \psi \frac{d^2 \mathcal{W}_m}{d\varepsilon^2} + \frac{d\psi}{dw}\frac{dw}{d\varepsilon}\sigma_m \tag{36}$$

Since during damage evolution $W = w$ —note that the form of this tangent is more similar shape to that of the CDM theory

$$E_T = \psi E_m + \frac{d\psi}{dw}\psi \sigma_m \sigma_m \tag{37}$$

During unloading–reloading, the tangent modulus is the elastic one, i.e. the one for $\dot{\psi} = 0$ which is $E = \psi E_m$. Then we can write in this case

$${}^{tr}\dot{\sigma} = \left.\frac{\partial^2 W(\varepsilon, w)}{\partial \varepsilon^2}\right|_{\dot{\psi}=0} \dot{\varepsilon} = \psi E_m \dot{\varepsilon} = E\dot{\varepsilon} \tag{38}$$

In incremental form, from step t to $t + \Delta t$ we can assume an elastic predictor increment—we use ${}^t\psi$ because ψ is assumed frozen during the substep

$$\Delta^{tr}\sigma = {}^tE\Delta\varepsilon = {}^t\psi E_m \Delta\varepsilon \tag{39}$$

Since during damage evolution $\dot{\sigma} = E_T\dot{\varepsilon}$, then

$${}^{t+\Delta t}\sigma = {}^t\sigma + E_T\Delta\varepsilon \tag{40}$$

by comparison with Eq. (35) we have that the corrector rate is

$${}^{ct}\dot{\sigma} = \left[\frac{d\psi}{d\varepsilon}\sigma_m\right]\dot{\varepsilon} \tag{41}$$

To obtain the incremental form we note that during this substep ε is frozen, so ${}^{t+\Delta t}\sigma_m \equiv {}^{tr}\sigma_m = E_m\, {}^{t+\Delta t}\varepsilon$ remains constant during the corrector substep, where only w (or equivalently ψ) changes. Thus

$$\Delta^{ct}\sigma = \Delta\psi\, {}^{t+\Delta t}\sigma_m = -\Delta L \tag{42}$$

with $\Delta\psi := {}^{t+\Delta t}\psi - {}^t\psi$. Then, the final stress adding both substeps (i.e. the effects of both partial derivatives)

$$\begin{aligned} {}^{t+\Delta t}\sigma &= {}^t\sigma + \Delta^{tr}\sigma + \Delta^{ct}\sigma = {}^t\sigma + \Delta^{tr}\sigma - \Delta L \\ &= {}^t\sigma + {}^t\psi E_m \Delta\varepsilon + \Delta\psi\, {}^{t+\Delta t}\sigma_m \end{aligned} \tag{43}$$

This is obviously a nonlinear equation in the general case because ${}^{t+\Delta t}\psi$ must fulfill the consistency condition ${}^{t+\Delta t}f = 0$. It is instructive to derive this equation at the converged $t + \Delta t$ to obtain the algorithmic tangent modulus

$$\begin{aligned} \frac{d\, {}^{t+\Delta t}\sigma}{d\, {}^{t+\Delta t}\varepsilon} &= {}^t\psi E_m + \Delta\psi E_m + {}^{t+\Delta t}\sigma_m \frac{d^{t+\Delta t}\psi}{d^{t+\Delta t}\varepsilon} \\ &= {}^t\psi E_m + \frac{d^{t+\Delta t}\psi}{d^{t+\Delta t}\varepsilon}\, {}^{t+\Delta t}\sigma_m \end{aligned} \tag{44}$$

which is to be compared to the continuum one obtained in Eq. (35). In Fig. 4 we show the integration process during a step. We finally note that the case of initial non-rigid behavior is simply accounted for by a maximum finite value of $\psi_{\max}$ (instead of the limit value of $\psi_{\max} \to \infty$ for the rigid case).

2.3 One-Dimensional Infinitesimal Framework in Terms of the Elastic Stored Energy $\mathcal{W}$

If during damage evolution the stored energy $\mathcal{W}$ increases monotonically, then $\mathcal{W}$ may be used as a suitable damage variable. In this case we consider the dependency $\mathcal{W}(\not{\phi}, w_D(\psi(\varepsilon))$ where the damage variable is

$$w_D = \max_{\tau \in (-\infty, t]} \mathcal{W}(\tau) \tag{45}$$

The rate of this energy is

$$\dot{\mathcal{W}}(\varepsilon, w_D) = \frac{d\mathcal{W}}{d\varepsilon}\dot{\varepsilon} = \left.\frac{\partial \mathcal{W}}{\partial \varepsilon}\right|_{\dot{w}_D=0} \dot{\varepsilon} + \left.\frac{\partial \mathcal{W}}{\partial w_D}\right|_{\dot{\varepsilon}=0} \frac{dw_D}{d\varepsilon}\dot{\varepsilon} \tag{46}$$

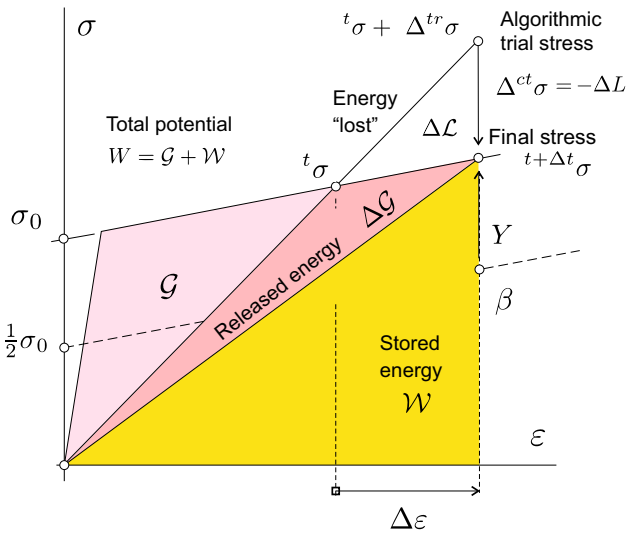

Fig. 4 Stress-like quantities involved during a step

The damage evolution condition Eq. (7) may be alternatively written as

$$f := W - w \equiv (\mathcal{W} + \mathcal{G}) - (w_D + \mathcal{G}) = \mathcal{W} - w_D \leq 0 \tag{47}$$

where $\mathcal{G}$ is the released elastic energy, see Eq. (5). We can of course invert $w_D(\psi)$ and write $\psi(w_D)$, and then write the elastic stored energy as $\mathcal{W}(\varepsilon, \psi(w_D(\varepsilon)))$. Then, using Eq. (9)

$$\left.\frac{\partial \mathcal{W}}{\partial \varepsilon}\right|_{\dot{w}_D=0} = \psi \frac{d\mathcal{W}_m}{d\varepsilon} = \sigma \tag{48}$$

Then, using Eqs. (5) and (9) during loading in the primary curve

$$\frac{dW}{d\varepsilon} = \psi \frac{d\mathcal{W}_m}{d\varepsilon} + \frac{d\psi}{d\varepsilon}\mathcal{W}_m + \frac{d\mathcal{G}}{d\varepsilon} \tag{49}$$

Since during loading in the primary curve $\sigma = \psi\sigma_m$, we have upon substitution in the previous equation that the last two terms must vanish

$$\frac{d\mathcal{G}}{d\varepsilon} = -\frac{d\psi}{d\varepsilon}\mathcal{W}_m := Y \tag{50}$$

We define—recall Eq. (9)

$$\gamma = -\left.\frac{\partial \mathcal{W}}{\partial w_D}\right|_{\dot{\varepsilon}=0} = -\left.\frac{\partial \mathcal{W}}{\partial \psi}\right|_{\dot{\varepsilon}=0}\frac{d\psi}{dw_D} = -\mathcal{W}_m\frac{d\psi}{dw_D} \tag{51}$$

as the energy release *ratio*. Then

$$\begin{aligned}\dot{\mathcal{W}} &= \dot{W} - \dot{\mathcal{G}} = \frac{dW}{d\varepsilon}\dot{\varepsilon} - \frac{d\mathcal{G}}{d\varepsilon}\dot{\varepsilon} \\ &= \sigma\dot{\varepsilon} - Y\dot{\varepsilon} = \beta\dot{\varepsilon} = \frac{d\mathcal{W}}{d\varepsilon}\dot{\varepsilon}\end{aligned} \tag{52}$$

We herein name the stress

$$\beta := \frac{d\mathcal{W}}{d\varepsilon} = \frac{d(\psi\mathcal{W}_m)}{d\varepsilon} = \psi\sigma_m + \frac{d\psi}{d\varepsilon}\mathcal{W}_m = \sigma - Y \tag{53}$$

as the *damage backstress*. For the bilinear case used as an example, from Eq. (16) we obtain for the case of damage evolution, after a little algebra

$$\beta = \tfrac{1}{2}\sigma_0 + E_T\varepsilon_u \Longrightarrow \dot{\beta} = E_T\dot{\varepsilon}_u \tag{54}$$

The energy release rate is

$$Y = \sigma - \beta = -\frac{d\psi}{d\varepsilon}\mathcal{W}_m = \gamma\frac{dw_D}{d\varepsilon} = \frac{1}{2}\sigma_0 \tag{55}$$

These quantities are depicted in Fig. 4 in the context of the bilinear model. Note that by comparison of Eqs. (46) and (52), using Eq. (51) we obtain

$$Y = \gamma\beta = -\left.\frac{\partial \mathcal{W}}{\partial \psi}\right|_{\dot{\varepsilon}=0}\frac{d\psi}{dw_D}\beta \tag{56}$$

$$Y = \gamma\beta = -\mathcal{W}_m\frac{d\psi}{dw_D}\beta = \frac{-\psi\mathcal{W}_m\dfrac{d\psi}{dw_D}}{1 - \mathcal{W}_m\dfrac{d\psi}{dw_D}}\sigma_m \tag{57}$$

Then, since during damage evolution $f = 0$ and $\dot{f} = 0$, from Eqs. (46) and (47) we obtain

$$\beta \equiv \frac{d\mathcal{W}}{d\varepsilon} \equiv \frac{dw_D}{d\varepsilon} = \frac{\psi}{1 - \mathcal{W}_m\dfrac{d\psi}{dw_D}}\sigma_m \tag{58}$$

The derivative of the stress is the tangent modulus, which during damage results in

$$E_T = \frac{d\sigma}{d\varepsilon} = \frac{d^2W}{d\varepsilon^2} = \frac{d}{d\varepsilon}\left(\psi\frac{d\mathcal{W}_m}{d\varepsilon}\right) \tag{59}$$

$$E_T = \psi\frac{d^2\mathcal{W}_m}{d\varepsilon^2} + \frac{d\psi}{dw_D}\frac{dw_D}{d\varepsilon}\frac{d\mathcal{W}_m}{d\varepsilon} \tag{60}$$

i.e. using Eq. (58)

$$E_T = \psi\frac{d^2\mathcal{W}_m}{d\varepsilon^2} + \frac{\psi\dfrac{d\psi}{dw_D}}{1 - \mathcal{W}_m\dfrac{d\psi}{dw_D}}\frac{d\mathcal{W}_m}{d\varepsilon}\frac{d\mathcal{W}_m}{d\varepsilon} \tag{61}$$

$$E_T = \psi E_m + \frac{\psi\dfrac{d\psi}{dw_D}}{1 - \mathcal{W}_m\dfrac{d\psi}{dw_D}}\sigma_m\sigma_m \tag{62}$$

Note that by comparison of this equation with Eq. (37) we obtain the relationship between $\psi(w)$ and $\psi(w_D)$

$$\frac{d\psi}{dw} = \frac{1}{w_D' - \mathcal{W}_m} \tag{63}$$

where $w_D' = dw_D/d\psi$. Using the $\mathcal{W}$-formulation, the trial stress concept may also be employed, see Eq. (38)

$${}^{tr}\dot{\sigma} = \left.\frac{\partial \sigma}{\partial \varepsilon}\right|_{\psi=0}\dot{\varepsilon} = \psi\frac{d^2W(\varepsilon, w)}{\partial\varepsilon^2}\dot{\varepsilon} = \psi E_m\dot{\varepsilon} \tag{64}$$

Hence $\dot{\sigma} = {}^{tr}\dot{\sigma} + {}^{ct}\dot{\sigma}$ results in

$$\underbrace{E_T\dot{\varepsilon}}_{\dot{\sigma}} = \underbrace{\psi E_m\dot{\varepsilon}}_{{}^{tr}\dot{\sigma}} + \underbrace{\frac{\psi}{w_D' - \mathcal{W}_m}\sigma_m\sigma_m\dot{\varepsilon}}_{{}^{ct}\dot{\sigma}} \tag{65}$$

However, in this framework it is better to work in a different way because in the previous equation the energy $\mathcal{W}_m$ appears explicitly. From Eq. (47), using $f = f(\varepsilon, \psi)$, since $\dot{f} = 0$ during damage evolution

$$\dot{f} = \dot{f}\big|_{\dot{\psi}=0} + \dot{f}\big|_{\dot{\varepsilon}=0} = {}^{tr}\dot{f} + {}^{ct}\dot{f} = 0 \tag{66}$$

where ${}^{tr}\dot{f} = \psi \mathcal{W}_m$ and ${}^{ct}\dot{f} = \mathcal{W}_m \dot{\psi} - w'_D \dot{\psi}$. Then, an incremental step brings the incremental equations

$$\Delta^{tr} f = {}^{t}\psi[\mathcal{W}_m({}^{t+\Delta t}\varepsilon) - \mathcal{W}_m({}^{t}\varepsilon)] \tag{67}$$

where note that we have used ${}^{t}\psi$ because in this substep damage is frozen, and

$$\Delta^{ct} f = [\mathcal{W}_m({}^{t+\Delta t}\varepsilon) - {}^{t+\Delta t}w'_D]\Delta\psi \tag{68}$$

with $\Delta\psi := ({}^{t+\Delta t}\psi - {}^{t}\psi)$. Then, $\Delta f = 0$ implies

$$\Delta f \equiv {}^{t+\Delta t}\psi \mathcal{W}_m({}^{t+\Delta t}\varepsilon) - {}^{t}\psi \mathcal{W}_m({}^{t}\varepsilon) - \Delta\psi\, {}^{t+\Delta t}w'_D = 0 \tag{69}$$

which is a nonlinear equation to be solved for ${}^{t+\Delta t}\psi$, for example using a Newton–Raphson method. Once this value is obtained, it is immediate to obtain the stress

$${}^{t+\Delta t}\sigma = {}^{t+\Delta t}\psi \frac{d\mathcal{W}_m({}^{t+\Delta t}\varepsilon)}{d^{t+\Delta t}\varepsilon} \tag{70}$$

The tangent modulus is

$$\frac{d^{t+\Delta t}\sigma}{d^{t+\Delta t}\varepsilon} = {}^{t+\Delta t}\psi \frac{d^2\mathcal{W}_m({}^{t+\Delta t}\varepsilon)}{d^{t+\Delta t}\varepsilon^2} + \frac{d\mathcal{W}_m({}^{t+\Delta t}\varepsilon)}{d^{t+\Delta t}\varepsilon} \frac{d^{t+\Delta t}\psi}{d^{t+\Delta t}\varepsilon} \tag{71}$$

The derivative of ${}^{t+\Delta t}\psi$ can be obtained from the derivative of the consistency condition

$$f = {}^{t+\Delta t}\psi \mathcal{W}_m({}^{t+\Delta t}\varepsilon) - w_D({}^{t+\Delta t}\psi) = 0 \tag{72}$$

so $df/d\varepsilon = 0$ results in

$$\frac{d^{t+\Delta t}\psi}{d^{t+\Delta t}\varepsilon} = \frac{{}^{t+\Delta t}\psi}{{}^{t+\Delta t}w'_D - {}^{t+\Delta t}\mathcal{W}_m} {}^{t+\Delta t}\sigma_m \tag{73}$$

Therefore

$$\begin{aligned}\frac{d^{t+\Delta t}\sigma}{d^{t+\Delta t}\varepsilon} = {}& {}^{t+\Delta t}\psi \frac{d^2\mathcal{W}_m({}^{t+\Delta t}\varepsilon)}{d^{t+\Delta t}\varepsilon^2} \\ & + \frac{{}^{t+\Delta t}\psi}{{}^{t+\Delta t}w'_D - {}^{t+\Delta t}\mathcal{W}_m} {}^{t+\Delta t}\sigma_m \, {}^{t+\Delta t}\sigma_m\end{aligned} \tag{74}$$

which is the same as that obtained in Eq. (62) after inverting the relation $\psi(w_D)$ to $w_D(\psi)$.

The development of a three-dimensional infinitesimal theory following these lines is straightforward and it may be considered a particular case of the large strain case if WYPiWYG hyperelasticity is employed. Hence, we address directly the large strain formulation based on WYPiWYG hyperelasticity.

3 WYPiWYG Hyperelasticity

Consider the polar decomposition of the deformation gradient $\boldsymbol{X}$ and the logarithmic strains

$$\boldsymbol{X} = \boldsymbol{R}\boldsymbol{U} \text{ and } \boldsymbol{E} = \ln \boldsymbol{U} \tag{75}$$

where $\boldsymbol{U}$ is the stretch tensor and $\boldsymbol{R}$ is the rotation one. WYPiWYG isotropic hyperelasticity for incompressible materials is based on the well-accepted Valanis–Landel decomposition of the form

$$\mathcal{W}(\boldsymbol{E}) = \omega(E_1) + \omega(E_2) + \omega(E_3) \tag{76}$$

where E_i are the principal logarithmic strains. Note that in the incompressible case, the volumetric strains vanish and $E_i^d = E_i$, where E_i^d are the isochoric logarithmic principal strains. The special properties of logarithmic strains [91, 92], which are parallel to those of the infinitesimal ones [87] are the reason why WYPiWYG procedures are based on those strains.

Consider for simplicity of the exposition the equilibrium equations of a tensile test in direction 1 for an incompressible material

$$\begin{cases} \sigma_1 = \tau_1 = T_1 = \omega'(E_1) - p \\ 0 = \omega'(E_2) - p \\ 0 = \omega'(E_3) - p \end{cases} \tag{77}$$

where $\boldsymbol{\sigma}$, $\boldsymbol{\tau}$, and $\boldsymbol{T}$ are, respectively, the Cauchy stresses, the Kirchhoff stresses and the generalized Kirchhoff stresses. These tensors are coincident in the isotropic incompressible case. Since by incompressibility $E_1 + E_2 + E_3 = 0$, we can factor-out the pressure-like lagrangian and obtain

$$\sigma_1(E_1) = \omega'(E_1) - \omega'\left(-\tfrac{1}{2}E_1\right) \tag{78}$$

where $\omega'(E)$ is the derivative of ω respect to E. Kearsley and Zapas [93] gave an explicit solution of this functional equation, which is called the inversion formula because it inverts the functional dependencies, i.e. from $\sigma(\omega'(E))$ to $\omega'(\sigma(E))$

$$\omega'(E_1) = \omega'(0) + \sum_{k=0}^{\infty} \sigma_1\left(-\frac{1}{2}\right)^k E_1 \tag{79}$$

We can take as a reference $\omega'(0) = 0$. The series coverges to machine precision in a finite number of terms, typically $20 - 50$. Then, given some experimental data $\{\tilde{E}_i, \tilde{\sigma}_i\}$, $i = 1, ..., N$, where N is the number of experimental points (say 100), the solution $\omega'(\tilde{E}_i)$ may be exactly obtained (to machine precision). Obviously if we want to do finite element analysis, a function $\omega'(E)$ is required. Then a proper interpolation may be performed between that experimental data in order to obtain a smooth function. In fact, in order

to apply Eq. (79) an interpolation between experimental data is also needed because σ_1 is evaluated at points different from the actual experimental points. We note that once $\omega'(E)$ has been obtained, it is of course valid in any loading situation and it can be applied to finite element analysis in a straightforward manner. The stresses and tangent moduli are obtained as in any other hyperelastic material upon knowledge of $\omega'(E) \equiv \omega'(E^d)$.

The WYPiWYG isotropic, incompressible model of Sussman and Bathe [78] made use of the Valanis–Landel decomposition and of the Kearsley and Zapas formula. In order to generalize the approach to compressible materials, transversely isotropic materials and orthotropic materials, we developed a generalization of the inversion formula in ref. [79]. Motivated in the infinitesimal setting we proposed the following Valanis–Landel-type decomposition for transversely isotropic materials [79]

$$\mathcal{W} = \omega_{11}(E_{11}) + \omega_{22}(E_{22}) + \omega_{33}(E_{33}) + 2\omega_{13}(E^{\#}_{13}) \tag{80}$$

and the following one for orthotropic materials [87]

$$\begin{aligned}\mathcal{W} = {} & \omega_{11}(E_{11}) + \omega_{22}(E_{22}) + \omega_{33}(E_{33}) \\ & + 2\omega_{13}(E_{13}) + 2\omega_{23}(E_{23}) + 2\omega_{12}(E_{12})\end{aligned} \tag{81}$$

where $\boldsymbol{a}_i$ are the principal material directions, $E_{ij} = \boldsymbol{a}_i \cdot \boldsymbol{E} \cdot \boldsymbol{a}_j$ are the components of the stress tensor in that preferred system of representation (i.e. they are invariants), $\boldsymbol{a}_3$ is the preferred direction in the transversely isotropic case and

$$E^{\#}_{13} = \sqrt{E^2_{13} + E^2_{23}} \tag{82}$$

is the shear invariant for the transversely isotropic case. We note that we are only neglecting the coupling invariant $E_{12}E_{13}E_{23}$ whose influence, in any case, would be difficult to characterize experimentally. In practice, if material symmetries are to be guaranteed [20], or (quasi-) compressibility accounted for [80], the following decomposition is to be enforced for the orthotropic case:

$$\mathcal{W}^{or}(\boldsymbol{E}) = \mathcal{W}^{is}(\boldsymbol{E}) + \tilde{\mathcal{W}}^{or}(\boldsymbol{E}) \tag{83}$$

where $\mathcal{W}^{is}$ is the isotropic contribution and $\tilde{\mathcal{W}}^{or}$ is the deviation from isotropy.

WYPiWYG hyperelasticity has some remarkable properties when compared to usual hyperelastic models. (1) Once the stored energy decomposition is assumed, the actual shape of the stored energy function is not specified but numerically computed from experimental data; (2) there are no material parameters and, hence, no optimization algorithms to obtain them; (3) they are compatible with the small strain theory at all deformation levels; (4) they capture, to machine precision if desired, as many complete experimental curves as material parameters used in the linear theory (i.e. their evolution) and (5) their numerical efficiency in finite element simulations is similar to that of traditional phenomenological models.

The reader is referred to refs. [79, 80, 87] for further information on WYPiWYG hyperelasticity, and to [84, 85] for WYPiWYG anisotropic viscoelasticity based on non-equilibrium thermodynamics. A fully coupled, general proposal for the stored energy is possible using the general procedure without inversion formula [81], but the determination of such a general stored energy implies elaborate experimental testing, so it may not be practical since coupling terms may be relevant only at very large strains. From now on, we assume that the WYPiWYG stored energy function captures exactly a master unloading–reloading $\mathcal{W}$ curve. Obviously the procedure could be used to also capture W; we will do so in the examples section to compare results.

4 WYPiWYG Isotropic Damage Mechanics

4.1 Continuum Theory

Considering that the stored energy increases until fracture, w_D is a suitable variable for tracking damage evolution. In the geometrically nonlinear case, we assume that the stored energy is given by

$$\Psi(\boldsymbol{E}, \psi) = \mathcal{U}(E^v) + \mathcal{W}\big(\boldsymbol{E}^d, \psi\left(w_D\right)\big) \tag{84}$$

where $\mathcal{U}(E^v)$ is the penalty volumetric energy and $E^v = \ln(\det(\boldsymbol{X}))$ is the volumetric logarithmic strain. In the isotropic case it can be shown that the hypothesis of the Valanis–Landel decomposition implies also

$$\mathcal{W}\big(\boldsymbol{E}^d, \psi(w_D)\big) = \psi(w_D)\mathcal{W}_m\big(\boldsymbol{E}^d\big) \tag{85}$$

i.e.

$$\begin{aligned}\mathcal{W}\big(\boldsymbol{E}^d, \psi(w_D)\big) = {} & \omega(E^d_1, \psi(w_D)) \\ & + \omega(E^d_2, \psi(w_D)) + \omega(E^d_3, \psi(w_D))\end{aligned} \tag{86}$$

$$\begin{aligned}\mathcal{W}\big(\boldsymbol{E}^d, \psi(w_D)\big) = {} & \psi(w_D)\omega_m(E^d_1) \\ & + \psi(w_D)\omega_m(E^d_2) + \psi(w_D)\omega_m(E^d_3)\end{aligned} \tag{87}$$

where $\psi(w_D)$ is the scalar function of the selected damage variable w_D

$$w_D = \max_{\tau\in(-\infty,t]} \mathcal{W}(\tau) \tag{88}$$

and $\omega_m(E^d_i)$ are the Valanis–Landel terms of the master hyperelastic curve as function of the isochoric principal logarithmic strains E^d_i. However we note that if Eq. (85) is assumed as usually done in isotropy, the present

formulation is valid even if the Valanis–Landel decomposition is not fulfilled. As a direct consequence of definition Eq. (88)

$$f = \mathcal{W} - w_D \leq 0 \tag{89}$$

During loading in the primary curve, damage is evolving and

$$f = 0 \text{ and } \dot{f} = 0 \Longleftrightarrow \dot{w}_D = \dot{\mathcal{W}} \tag{90}$$

Then, for the nontrivial case in which $\dot{\boldsymbol{E}}^d \neq \boldsymbol{0}$, $\dot{f} = 0$ results in

$$\frac{\partial \mathcal{W}(\boldsymbol{E}^d, \psi)}{\partial \boldsymbol{E}^d} + \frac{\partial \mathcal{W}(\boldsymbol{E}^d, \psi)}{\partial \psi} \frac{d\psi}{dw_D} \frac{dw_D}{d\boldsymbol{E}^d} - \frac{dw_D}{d\boldsymbol{E}^d} = 0 \tag{91}$$

Using Eqs. (85) and (91) is

$$\psi \frac{d\mathcal{W}_m}{d\boldsymbol{E}^d} + \mathcal{W}_m \frac{d\psi}{dw_D} \frac{dw_D}{d\boldsymbol{E}^d} - \frac{dw_D}{d\boldsymbol{E}^d} = 0 \tag{92}$$

Since the generalized Kirchhoff stresses are work-conjugate to the material logarithmic strains in the most general anisotropic case, during primary loading the following generalized Kirchhoff stress tensor [94] may be defined—cf. Eq. (49)

$$\begin{aligned} \boldsymbol{T}^{|d} &= \frac{dW(\boldsymbol{E}^d, \psi)}{d\boldsymbol{E}^d} = \frac{d\mathcal{W}}{d\boldsymbol{E}^d} + \frac{d\mathcal{G}}{d\boldsymbol{E}^d} \\ &= \psi \frac{d\mathcal{W}_m}{d\boldsymbol{E}^d} + \frac{d\mathcal{G}}{d\boldsymbol{E}^d} + \mathcal{W}_m \frac{d\psi}{dw_D} \frac{dw_D}{d\boldsymbol{E}^d} \end{aligned} \tag{93}$$

where $(\cdot)^{|d}$ stands for derivative having been taken respect to the deviatoric strains. However, we also have

$$\boldsymbol{T}^{|d} = \psi \frac{d\mathcal{W}_m}{d\boldsymbol{E}^d} = \frac{\partial \mathcal{W}}{\partial \boldsymbol{E}^d} \tag{94}$$

Hence—cf. Eq. (50)

$$\boldsymbol{Y} = \frac{d\mathcal{G}}{d\boldsymbol{E}^d} = -\mathcal{W}_m \frac{d\psi}{dw_D} \frac{dw_D}{d\boldsymbol{E}^d} = :\gamma \boldsymbol{B} \tag{95}$$

where—cf. Eq. (53)

$$\boldsymbol{B} = \frac{dw_D}{d\boldsymbol{E}^d} = \psi \frac{d\mathcal{W}_m}{d\boldsymbol{E}^d} + \mathcal{W}_m \frac{d\psi}{dw_D} \frac{dw_D}{d\boldsymbol{E}^d} = \frac{\psi w_D'}{w_D' - \mathcal{W}_m} \boldsymbol{T}_m^{|d} \tag{96}$$

with the reference stress

$$\boldsymbol{T}_m^{|d} := \frac{d\mathcal{W}_m}{d\boldsymbol{E}^d} \tag{97}$$

Then—cf. Eqs. (53) and (55)

$$\boldsymbol{T}^{|d} = \boldsymbol{B} + \boldsymbol{Y} \tag{98}$$

Alternatively, we can also define

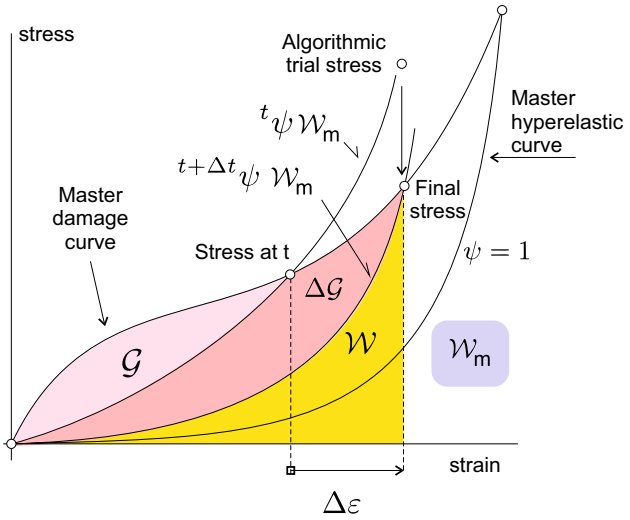

Fig. 5 Energies involved in a step in the nonlinear case

$$^{tr}\boldsymbol{T}^{|d} := \frac{\partial W}{\partial \boldsymbol{E}^d} = \frac{dW}{d\boldsymbol{E}^d} - \frac{dW}{dw} \frac{dw}{d\boldsymbol{E}^d} = \boldsymbol{T}^{|d} + \boldsymbol{L} \tag{99}$$

so we have—cf. Eq. (28)

$$\boldsymbol{T}^{|d} = {}^{tr}\boldsymbol{T}^{|d} + {}^{ct}\boldsymbol{T}^{|d} = {}^{tr}\boldsymbol{T}^{|d} - \boldsymbol{L} \text{ with } \boldsymbol{L} = -\frac{dW}{dw} \frac{dw}{d\boldsymbol{E}^d} \tag{100}$$

Hence, no relevant change respect to the one-dimensional bi-linear case is present. The energies involved in the nonlinear case are shown in Fig. 5.

4.2 Algorithmic Formulation

The numerical algorithm based on the $\mathcal{W}$–formulation is also very similar to that of the one-dimensional infinitesimal problem. As shown in Fig. 5, the objective is to find the value of ψ for which

$$f := \psi \mathcal{W}_m - w_D = 0 \tag{101}$$

In incremental form, the trial value is given for $\Delta\psi = 0$ and the new value of $^{t+\Delta t}\boldsymbol{E}$

$$^{tr}f = {}^t\psi \mathcal{W}_m\left({}^{t+\Delta t}\boldsymbol{E}^d\right) - {}^t w_D \tag{102}$$

If $^{tr}f > 0$, then damage evolution takes places, i.e. the values of $^t\psi$ and $^t w_D$ need to be updated performing the proper correction

$$^{ct}f = ({}^{t+\Delta t}\psi - {}^t\psi)\mathcal{W}_m\left({}^{t+\Delta t}\boldsymbol{E}^d\right) - ({}^{t+\Delta t}w_D - {}^t w_D) \tag{103}$$

Then, the nonlinear *scalar* equation is

$$^{t+\Delta t}f = {}^{t+\Delta t}\psi \mathcal{W}_m\left({}^{t+\Delta t}\boldsymbol{E}^d\right) - {}^{t+\Delta t}w_D = 0 \tag{104}$$

which can be immediately solved using, for example, a Newton–Raphson procedure, i.e.

$$ {}^{t+\Delta t}\psi^{(j+1)} = {}^{t+\Delta t}\psi^{(j)} - \left[\frac{d^{t+\Delta t}f^{(j)}}{d^{t+\Delta t}\psi^{(j)}}\right]^{-1} {}^{t+\Delta t}f^{(j)} \tag{105} $$

where

$$ \frac{\partial^{t+\Delta t}f^{(j)}}{\partial^{t+\Delta t}\psi^{(j)}} = \mathcal{W}_m\left({}^{t+\Delta t}\boldsymbol{E}^d\right) - w_D'({}^{t+\Delta t}\psi) \tag{106} $$

Since $\mathcal{W}_m\left({}^{t+\Delta t}\boldsymbol{E}^d\right)$ is the known WYPiWYG master stored energy and $w_D({}^{t+\Delta t}\psi)$ has been previously obtained from the master primary loading and unloading–reloading curves, this derivative is readily computed. The starting values are obviously ${}^{t+\Delta t}\psi = {}^{t}\psi$ and ${}^{t+\Delta t}f^{(0)} = {}^{tr}f$.

Once ${}^{t+\Delta t}\psi$ has been computed, the value for the stresses is

$$ {}^{t+\Delta t}\boldsymbol{T} = \mathcal{U}'({}^{t+\Delta t}E^v)\boldsymbol{I} + {}^{t+\Delta t}\psi\ {}^{t+\Delta t}\boldsymbol{T}_m^{|d}:\mathbb{P}^d \tag{107} $$

where $\mathcal{U}'({}^{t+\Delta t}E^v)$ is the derivative of the penalty function for the volumetric constraint. The tensor $\mathbb{P}^d = d\boldsymbol{E}^d/d\boldsymbol{E}$ is the usual deviatoric projector tensor for logarithmic and infinitesimal strains, so for example $\boldsymbol{T}^d = \boldsymbol{T}^{|d}:\mathbb{P}^d$ are the deviatoric stresses.

The constitutive tangent may be obtained by direct differentation

$$ \begin{aligned} \mathbb{C}_T^{|d} &= \frac{d\,{}^{t+\Delta t}\boldsymbol{T}^{|d}}{d\,{}^{t+\Delta t}\boldsymbol{E}^d} = \frac{d({}^{t+\Delta t}\psi\ {}^{t+\Delta t}\boldsymbol{T}_m^{|d})}{d\,{}^{t+\Delta t}\boldsymbol{E}^d} \\ &= {}^{t+\Delta t}\psi\ {}^{t+\Delta t}\mathbb{C}_m^{|d} + {}^{t+\Delta t}\boldsymbol{T}_m^{|d} \otimes \frac{d\,{}^{t+\Delta t}\psi}{d\,{}^{t+\Delta t}\boldsymbol{E}^d} \end{aligned} \tag{108} $$

where

$$ {}^{t+\Delta t}\mathbb{C}_m^{|d} = \frac{d^2\,{}^{t+\Delta t}\mathcal{W}_m}{d^{t+\Delta t}\boldsymbol{E}^d\ d^{t+\Delta t}\boldsymbol{E}^d} \tag{109} $$

The tensor $d^{t+\Delta t}\psi/\ d^{t+\Delta t}\boldsymbol{E}^d$ vanishes in the case of unloading–reloading. In the case of damage evolution, this tensor may be computed from the consistency condition $\dot{f} = 0$ using Eq. (104)

$$ \begin{aligned} \frac{d\,{}^{t+\Delta t}f}{d\,{}^{t+\Delta t}\boldsymbol{E}^d} &= {}^{t+\Delta t}\mathcal{W}_m \frac{d\,{}^{t+\Delta t}\psi}{d\,{}^{t+\Delta t}\boldsymbol{E}^d} + {}^{t+\Delta t}\psi\ {}^{t+\Delta t}\boldsymbol{T}_m^{|d} \\ &\quad - w_D'({}^{t+\Delta t}\psi)\frac{d^{t+\Delta t}\psi}{d\,{}^{t+\Delta t}\boldsymbol{E}^d} = \boldsymbol{0} \end{aligned} \tag{110} $$

so

$$ \frac{d^{t+\Delta t}\psi}{d\,{}^{t+\Delta t}\boldsymbol{E}^d} = \frac{{}^{t+\Delta t}\psi}{w_D'({}^{t+\Delta t}\psi) - {}^{t+\Delta t}\mathcal{W}_m}\ {}^{t+\Delta t}\boldsymbol{T}_m^{|d} \tag{111} $$

and

$$ \mathbb{C}_T^{|d} = {}^{t+\Delta t}\psi\ {}^{t+\Delta t}\mathbb{C}_m^{|d} + {}^{t+\Delta t}\theta\ {}^{t+\Delta t}\boldsymbol{T}_m^{|d} \otimes {}^{t+\Delta t}\boldsymbol{T}_m^{|d} \tag{112} $$

with

$$ {}^{t+\Delta t}\theta = \begin{cases} \dfrac{{}^{t+\Delta t}\psi}{w_D'({}^{t+\Delta t}\psi) - {}^{t+\Delta t}\mathcal{W}_m} & \text{if } {}^{tr}f > 0 \\ 0 & \text{if } {}^{tr}f \le 0 \end{cases} \tag{113} $$

which is an expression which resembles that of classical CDM models. The full tangent is—we omit time-step indices

$$ \mathbb{C}_T = \mathcal{U}''(E^v)\boldsymbol{I}\otimes\boldsymbol{I} + \mathbb{P}^d:\mathbb{C}_T^{|d}:\mathbb{P}^d \tag{114} $$

This tangent may be readily converted to any other stress and strain measures through proper mapping tensors as described, for example, in ref. [94]. Further details are omitted herein. We note that alternatively, if ψ is expressed in terms of the maximum master value reached (e.g. $\psi(w_m)$ with $w_m = \max_{\tau\in(-\infty,t]}\mathcal{W}_m$), no local iterations are needed in the strain-driven case.

As we show in the examples below, WYPiWYG isotropic damage mechanics is capable of capturing to high accuracy both the primary loading curve and one unloading–reloading curve. The other ones, due to the assumptions of isotropy and Valanis–Landel decomposition must be proportional.

5 Anisotropic WYPiWYG Damage Mechanics

5.1 Continuum Theory

Isotropic damage is a convenient modelling assumption which is hardly found in actual materials. Isotropic damage assumes the same damage in all directions. For example, if after some damage, the same specimen is also uniaxially loaded in other directions up to the same level, no further damage will be predicted. Hence, only damage under uniaxial loading or damage in some materials as ductile metals, may be properly modeled with isotropic damage. In polymeric materials, damage can be considered isotropic only in the first stages. However, isotropic damage is frequently used as a simplifying convenient assumption because determining fully anisotropic damage evolution from experiments is a very complicated task. However, as already explained in the "Introduction" section, anisotropic damage is important for damage-induced anisotropy and for characterizing the anisotropic Mullins effect in soft biological tissues, which are mostly anisotropic.

The extension of damage models to include anisotropic damage goes necessarily through the consideration of more than one anisotropic damage variable. The number and type of damage variables to be employed has been a topic of active research in the 1970s and 1980s. For example in the work of Hayhurst and Leckie [95], the loading direction is included to characterize damage and in [96] a second order tensor to modify effective areas is proposed. Many other proposals may be found in [41]. However, in this work we follow the concepts given in [97] and [98] (among others) in which the strain energy itself (or equivalently in the linear case, the constitutive tensor) is used to model damage. We will herein address in detail the orthotropic case, since the transversely isotropic case is similar.

Because the most practical case of WYPiWYG orthotropic incompressible hyperelasticity is based on a decomposition of the form Eq. (81), six damage variables may be employed to modify each one of the terms in Eq. (81). Of course if material symmetries congruency is to be obtained, Eq. (83) is to be employed and an additional damage variable accounting for the isotropic part is considered. In such case, that variable considers the isotropic contribution of damage, whereas the other ones account for the anisotropic deviation.

In the formulation herein presented there is an inherent restriction. We assume that the material symmetry planes are preserved during all the deformation process, so an orthotropic material remains being orthotropic and keeping the same symmetry planes (the preferred directions in the reference configuration are the same). This is of course a simplifying hypothesis because damage in general is known to usually develop fully anisotropic behavior with no symmetry planes in the general case. However, this hypothesis will allow us to develop a tractable formulation and a procedure to determine the behaviour of transversely isotropic and orthotropic damaged materials, or when such anisotropies are developed due to damage. We will consider that the stored energy function may be written as

$$\Psi\left(\boldsymbol{E},\ \boldsymbol{w}_D\right) = \mathcal{U}(E^v) + \mathcal{W}\left(\boldsymbol{E}^d,\ \boldsymbol{w}_D\right) \tag{115}$$

For the isochoric component we consider a decomposition similar to that of Valanis and Landel

$$\begin{aligned}\mathcal{W}^{or}\left(\boldsymbol{E}^d, \boldsymbol{w}_D\right) = {} & \omega_{11}\left(E^d_{11}, w_{11D}\right) + \omega_{22}\left(E^d_{22}, w_{22D}\right) \\ & + \omega_{33}\left(E^d_{33}, w_{33D}\right) + 2\omega_{12}\left(E^d_{12}, w_{12D}\right) \\ & + 2\omega_{13}\left(E^d_{13}, w_{13D}\right) + 2\omega_{23}\left(E^d_{23}, w_{23D}\right)\end{aligned} \tag{116}$$

where $\boldsymbol{w}_D$ is the array of damage variables, the factor of two accounts for similar terms $\omega_{ij} \equiv \omega_{ji}$, and

$$E^d_{ij} = \boldsymbol{a}_i \cdot \boldsymbol{E}^d \cdot \boldsymbol{a}_j \tag{117}$$

are the components of the isochoric logarithmic strains in the principal material directions of orthotropy $\boldsymbol{a}_i$. In order to preserve the material-symmetries congruency [20], we add an isotropic contribution

$$\mathcal{W}\left(\boldsymbol{E}^d, \boldsymbol{w}_D\right) = \mathcal{W}^{is}\left(\boldsymbol{E}^d, w_D\right) + \mathcal{W}^{or}\left(\boldsymbol{E}^d, \boldsymbol{w}_D\right) \tag{118}$$

where w_D is the isotropic damage variable and $\boldsymbol{w}_D$ is a matrix of anisotropic ones. The meaning of the damage variables is taken as

$$\begin{cases} w_D(t) = \max\limits_{\tau\in(-\infty,t]} \mathcal{W}^{is}(\boldsymbol{E}^d(\tau), w_D(\tau)) \\ w_{ijD}(t) = \max\limits_{\tau\in(-\infty,t]} [\omega_{ij}(E^d_{ij}(\tau), w_{ijD}(\tau))] \\ \qquad \text{with } i \le j = 1,2,3 \end{cases} \tag{119}$$

Therefore, inherent to these definitions are those of the damage criteria

$$\begin{cases} f = \mathcal{W}^{is}(\boldsymbol{E}^d, w_D) - w_D \le 0 \\ f_{ij} = \omega_{ij}(E^d_{ij}, w_{ijD}) - w_{ijD} \le 0 \\ \qquad \text{with } i \le j = 1,2,3 \end{cases} \tag{120}$$

Since there are few further differences in the continuum structure to the isotropic case, we address directly the algorithm formulation.

5.2 Algorithmic Formulation

We have seen in previous sections that the isotropic component may be written as

$$\mathcal{W}^{is}(\boldsymbol{E}^d, w_D) = \psi(w_D)\mathcal{W}^{is}_m(\boldsymbol{E}^d) \tag{121}$$

which results into

$$\omega(E^d, w_D) = \psi(w_D)\text{ſ}_m(E^d) \tag{122}$$

where $\omega(E^d, w_D)$ is a reference hyperelastic function for a given damage level and ψ is the scaling function which is $\psi = 1$ for the reference damaged state characterized by ω_m . In this formulation, we proceed in a similar way with the orthotropic functions given in Eq. (116). Then, the following setting is a modelling assumption

$$\omega_{ij}(E^d_{ij}, w_{ijD}) = \psi_{ij}(w_{ijD})\omega_{mij}(E^d_{ij}) \tag{123}$$

which obviously brakes the proportionality of the global stored energy for the general case of orthotropy. In Eq. (123) the functions $\omega_{mij}(E^d_{ij})$ are the hyperelastic functions of the Valanis–Landel-type decomposition for a reference damage, whereas the functions $\psi_{ij}(w_{ijD})$ are the corresponding scaling functions.

As in the isotropic case, the main objective of the local algorithm is to determine the scaling factors ψ_{ij}, because once determined, the stresses are computed as in non-damaged hyperelasticity, simply by derivation of the strain energy as

$$\boldsymbol{T}^{|d} = \psi(w_D)\frac{d\mathcal{W}_m^{is}(\boldsymbol{E}^d)}{d\boldsymbol{E}^d} + \sum_{i,j}\psi_{ij}(w_{ijD})\frac{d\omega_{mij}(E_{ij}^d)}{d\boldsymbol{E}^d} \tag{124}$$

The first addend is the isotropic contribution, i.e.

$$\boldsymbol{T}^{is|d} = \psi(w_D)\frac{\partial\mathcal{W}_m^{is}(\boldsymbol{E}^d)}{d\boldsymbol{E}^d} \tag{125}$$

$$\boldsymbol{T}^{is|d} = \sum_{i,j}\psi(w_D)\frac{d\omega_m(E_i^d)}{dE_i^d}\boldsymbol{N}_i\otimes\boldsymbol{N}_i \tag{126}$$

where $\boldsymbol{N}_i$ are the principal directions of the right stretch tensor and E_i^d are the principal logarithmic strains. The other addends in Eq. (124) are the anisotropic deviations, where (no sum in repeated indices)

$$\boldsymbol{T}_{mij}^{|d} = \frac{d\omega_{mij}(E_{ij}^d)}{d\boldsymbol{E}^d} = \frac{d\omega_{mij}(E_{ij}^d)}{dE_{ij}^d}\frac{dE_{ij}^d}{d\boldsymbol{E}^d} \tag{127}$$

and E_{ij}^d are the strain components corresponding to the strain energy components ω_{mij}. Taking into account symmetries, these strains are computed as

$$E_{ij}^d = \frac{1}{2}(\boldsymbol{a}_i\cdot\boldsymbol{E}^d\cdot\boldsymbol{a}_j + \boldsymbol{a}_j\cdot\boldsymbol{E}^d\cdot\boldsymbol{a}_i) \tag{128}$$

so the strucural tensors are

$$\boldsymbol{L}_{ij} := \frac{dE_{ij}^d}{d\boldsymbol{E}^d} = \frac{1}{2}(\boldsymbol{a}_i\otimes\boldsymbol{a}_j + \boldsymbol{a}_j\otimes\boldsymbol{a}_i) \tag{129}$$

Assume that we know the function $\psi_{ij}(w_{ijD})$, or conversely $w_{ijD}(\psi_{ij})$. The strains at $t+\Delta t$, namely ${}^{t+\Delta t}\boldsymbol{E}$, and the values of the multiplier functions ${}^{t}\psi_{ij}$ allow for the computation of the trial consistency functions

$$\begin{cases} {}^{tr}f := {}^{t}\psi\mathcal{W}_m^{is}({}^{t+\Delta t}\boldsymbol{E}^d) - {}^{t}w_D \\ {}^{tr}f_{ij} := {}^{t}\psi_{ij}\mathcal{W}_{mij}({}^{t+\Delta t}E_{ij}^d) - {}^{t}w_{ijD} \end{cases} \tag{130}$$

We note that once ${}^{t+\Delta t}\boldsymbol{E}$ is given, these functions are independent to each other; the coupling is indirectly given by the strain tensor. For example a change in ψ_{11} does not change the other functions. Hence, the computation of the different ${}^{t+\Delta t}\psi_{ij}$ may be performed in a loop. The ψ_{ij} functions are uncoupled and each one only depends on the corresponding strain component in the principal material axis.

We can obtain directly ψ_{ij} if we build the spline function as $\psi_{ij}(w_{mij}(E_{ij}^d)) = \psi_{ij}(E_{ij}^d)$—note that this is a similar case as the one-dimensional one, see Eq. (16). For the isotropic part, the procedure is the same as that described in Section 4.2.

Once all proportionality parameters ψ_{ij} have been computed, the stress tensor is

$${}^{t+\Delta t}\boldsymbol{T} = \mathcal{U}'(E^v)\boldsymbol{I} + {}^{t+\Delta t}\boldsymbol{T}^{|d} : \mathbb{P}^d \tag{131}$$

where

$${}^{t+\Delta t}\boldsymbol{T}^{|d} = {}^{t+\Delta t}\psi\,{}^{t+\Delta t}\boldsymbol{T}_m^{|d} + \sum_{i,j}{}^{t+\Delta t}\psi_{ij}\,{}^{t+\Delta t}\boldsymbol{T}_{mij}^{|d} \tag{132}$$

The constitutive tangent may be obtained from Eq. (124)—all quantities are evaluated at the converged solution at $t+\Delta t$, so we omit the time-step index

$$\begin{aligned}\mathbb{C}_T^{|d} := \frac{d\boldsymbol{T}^{|d}}{d\boldsymbol{E}^d} &= \psi(w_D)\mathbb{C}_m^{is|d} + \boldsymbol{T}_m^{is|d}\otimes\frac{d\psi(w_D)}{d\boldsymbol{E}^d} \\ &+ \sum_{i,j}\psi_{ij}(w_{ijD})\mathbb{C}_{mij} \\ &+ \sum_{i,j}\frac{d\omega_{mij}(E_{ij}^d)}{d\boldsymbol{E}^d}\otimes\frac{d\psi_{ij}(w_{ijD})}{d\boldsymbol{E}^d}\end{aligned} \tag{133}$$

with

$$\mathbb{C}_m^{is|d} := \frac{d^2\mathcal{W}_m^{is}(\boldsymbol{E}^d)}{d\boldsymbol{E}^d d\boldsymbol{E}^d} \tag{134}$$

and (no sum on repeated indices)

$$\mathbb{C}_{mij}^{|d} = \frac{d^2\omega_{mij}(E_{ij}^d)}{d\boldsymbol{E}^d d\boldsymbol{E}^d} = \frac{d^2\omega_{mij}(E_{ij}^d)}{dE_{ij}^d dE_{ij}^d}\boldsymbol{L}_{ij}\otimes\boldsymbol{L}_{ij} \tag{135}$$

The tensor $d\psi_{ij}(w_{ijD})/d\boldsymbol{E}^d$ can be obtained from the corresponding consistency condition if ${}^{tr}f_{ij} \geq 0$, i.e.—no sum on i,j

$$\frac{df_{ij}}{d\boldsymbol{E}^d} = \psi\boldsymbol{T}_{mij}^{|d} + \omega_{mij}(E_{ij}^d)\frac{d\psi_{ij}}{d\boldsymbol{E}^d} - \frac{d\omega_{ijD}}{d\psi_{ij}}\frac{d\psi_{ij}}{d\boldsymbol{E}^d} = 0 \tag{136}$$

so

$$\frac{d\psi_{ij}}{d\boldsymbol{E}^d} = \theta_{ij}\boldsymbol{T}_{mij}^{|d} \tag{137}$$

where

$$\theta_{ij} := \begin{cases} \dfrac{\psi_{ij}}{d\omega_{ijD}/d\psi_{ij} - \omega_{mij}(E_{ij}^d)} & \text{if } {}^{tr}f > 0 \\ 0 & \text{if } {}^{tr}f = 0 \end{cases} \tag{138}$$

Therefore

$$\mathbb{C}_T^{|d} = \psi \mathbb{C}_m^{is|d} + \theta \boldsymbol{T}_m^{is|d} \otimes \boldsymbol{T}_m^{is|d} + \sum_{i,j} \left(\psi_{ij}(w_{ijD}) \mathbb{C}_{mij}^{|d} + \theta_{ij} \boldsymbol{T}_{mij}^{|d} \otimes \boldsymbol{T}_{mij}^{|d} \right) \tag{139}$$

and

$$\mathbb{C}_T = \mathcal{U}''(E^v) \boldsymbol{I} \otimes \boldsymbol{I} + \mathbb{P}^d : \mathbb{C}_T^{|d} : \mathbb{P}^d \tag{140}$$

This tensor can be mapped to the desired stress–strain conjugate pair using the deformation gradient. Remarkably, these expressions take a layout similar to that found in CDM models.

5.3 Extraction of the Information From Experiments

As we have already mentioned, six experimental data curves are required to obtain the different terms that are present in the isochoric strain energy function corresponding to the master damage curves and the master hyperelastic curves respectively. For the master damage curves three uniaxial loading tests up to the maximum strain level to be attained in the simulations, performed in the three preferred directions of the material on three identical material samples are needed to calculate the axial terms ω_{ii}, cf. [87]. As also explained therein the shear terms of the type ω_{ij}can be determined, for example, from three specific pure shear tests. On the other hand in order to obtain the axial terms of the energy function corresponding to the master hyperelastic curves, a simple sample is loaded up to the maximum strain expected in the simulations, for which the damage is maximum ($\psi_i = 1$), and once achieved, the specimen is unloaded. This is done in each of the three preferred directions successively. That is, the specimen will be subjected to a load and subsequent unload in the three preferred material directions in turn. The experimental data corresponding to the unloading in the third direction are the ones needed to obtain the axial terms corresponding to the master hyperelastic curves, again see ref. [87]. Note that by incompressibility, damage evolution in one direction is coupled with that in the transverse directions, unless we can assume that compression strains do not lead to damage in the corresponding direction (in the examples below we consider the more elaborated coupled case). Thereby this procedure is repeated three times permuting the preferred direction of the last test. Proceeding in a similar way, the shear terms are obtained as for the master damage curves, from three specific pure shear tests.

In the above-described procedure, the main information needed from experiments are the curves $w_{ijD}(\psi_{ij})$, $\omega_{mij}\left(E_{ij}^d\right)$ and $\mathcal{W}^{is}\left(\boldsymbol{E}^d\right)$. Unless there is some physical insight in the material being tested, it is difficult if not impossible to distinguish from uniaxial tests which part corresponds to the isotropic part and which one is the orthotropic contribution. If the nature of the material being tested is known, it could be the case that the isotropic contribution may be devised or determined (for example performing tests on the isolated matrix component or assuming that the behavior in one direction is mainly due to that component).

Now assume that we have determined the part that corresponds to isotropic behavior. To do so, we simply determine the unloading–reloading curve for isotropy and the corresponding master damage curve. Following the procedure detailed in [86] we obtain the functions $\mathcal{W}^{is}(\boldsymbol{E})$ (see [78, 87]) and $w_D(\psi)$. With these data, we can determine the isochoric isotropic contribution in the principal orthotropy directions, and perform the additive decomposition Eq. (118):

$$\mathcal{U} + \mathcal{W} = \mathcal{U} + \mathcal{W}^{is} + \mathcal{W}^{or} \Rightarrow \mathcal{W}^{or} = \mathcal{W} - \mathcal{W}^{is} \tag{141}$$

which in terms of stresses results, up to a common pressure lagrange multiplier, in

$$\boldsymbol{T}^{or}(\boldsymbol{E}) = \frac{\partial \mathcal{W}}{\partial \boldsymbol{E}} - \frac{\partial \mathcal{W}^{is}}{\partial \boldsymbol{E}} = \boldsymbol{T}^{d}(\boldsymbol{E}) - \boldsymbol{T}^{is}(\boldsymbol{E}) \tag{142}$$

Since for the six needed experiments $\boldsymbol{T}^d(\boldsymbol{E})$ is known and $\boldsymbol{T}^{is}(\boldsymbol{E})$ can be determined, then six curves corresponding to $\boldsymbol{T}^{or}(\boldsymbol{E})$ may be obtained. A general interpretation of all these quantities is given in Fig. 6. Furthermore, since

$$\boldsymbol{T}^{or}(\boldsymbol{E}) = \sum_{i,j} \psi_{ij}\left(w_{ijD}\right) \boldsymbol{T}_{mij}^{d}(\boldsymbol{E}) \tag{143}$$

the functions ω_{mij} are then determined directly from the (damaged) hyperelastic curve $\boldsymbol{T}_m^d(\boldsymbol{E}) - \boldsymbol{T}_m^{is}(\boldsymbol{E})$ assuming that both prescribed $\boldsymbol{T}_m^d(\boldsymbol{E})$ and $\boldsymbol{T}_m^{is}(\boldsymbol{E})$ curves correspond to the same level of damage (master hyperelastic curve). Then, the values of the multipliers ψ_{ij} are obtained from the already known multiplier ψ and the master damage curve for each direction

$$\psi_{ij} = \frac{T^d - \psi T_m^{is}}{T_{mij}^d} \tag{144}$$

where un-bold symbols imply that we are using the uniaxial values.

6 Examples

6.1 One-Dimensional, Infinitesimal Bilinear Example

As a demonstrative example to explain the concepts in the simplest possible context, we consider a bilinear material at small strains. Assume that the hypothetical material is

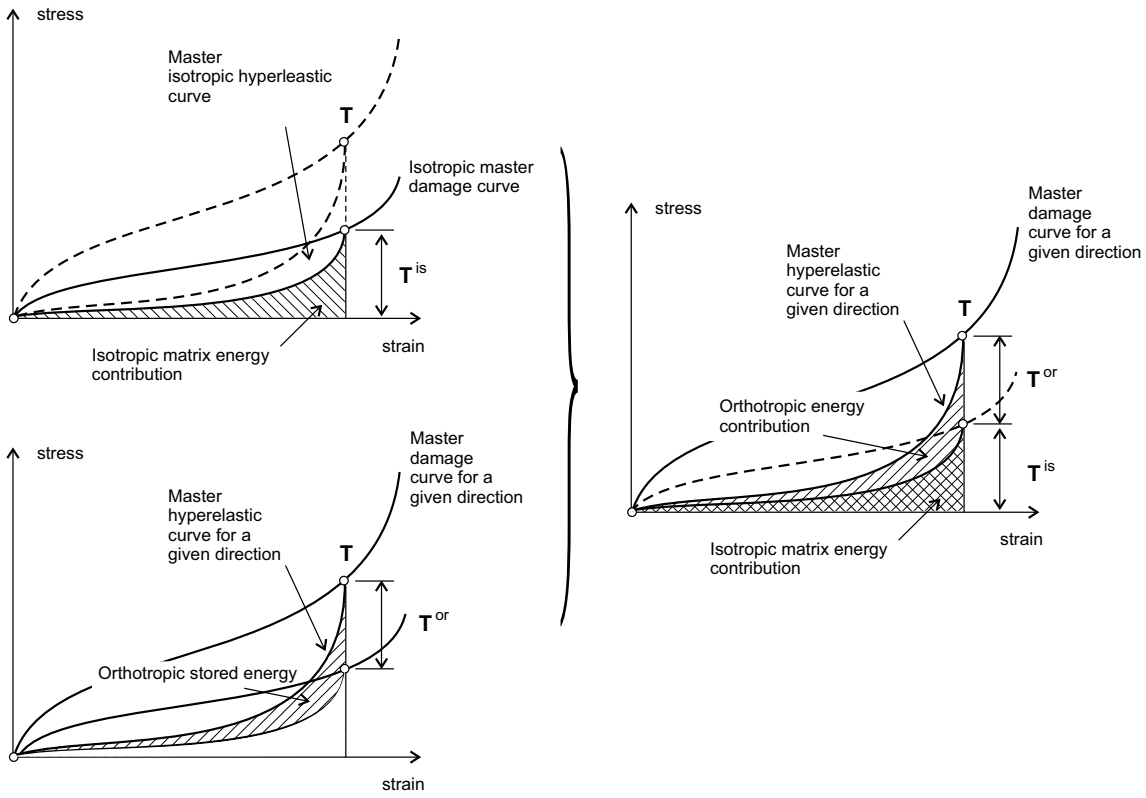

Fig. 6 Schematic representation of the orthotropic and isotropic contributions to total stress

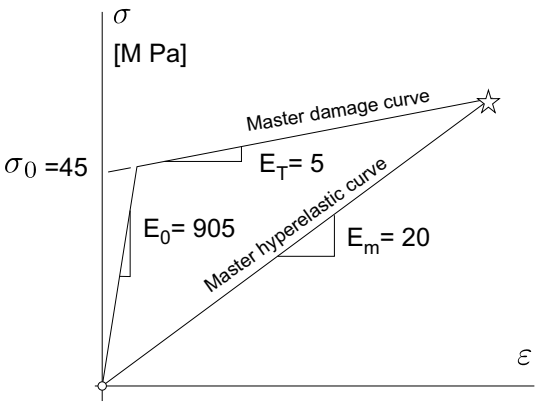

Fig. 7 Prescribed experimental data for theoretical bilinear example

defined by a master damage curve and a master hyperelastic curve as can be observed in Fig. 7.

Performing a tensile test in the longitudinal direction and loading and unloading at different load levels, it can be observed that the stress–strain data predicted by the algorithm matches exactly the prescribed data, see Fig. 8a, b. For example, assume we first stretch the material to a maximum strain $\varepsilon_u = 2$, during loading according to Eq. (15) we obtain,

$$\psi(\varepsilon_u) = \frac{\sigma_0 + E_T\varepsilon_u}{E_m\varepsilon_u} = \frac{45 + 5\times 2}{20\times 2} = 1.375 \tag{145}$$

Then, the following results may be immediately computed from the above expressions and verified geometrically in Fig. 8a

$$\begin{cases} \sigma = \psi\sigma_m = \psi E_m\varepsilon_u = 55\text{MPa} \\ \mathcal{W}(\varepsilon_u,\psi) = w_D(\varepsilon_u) = \psi\mathcal{W}_m(\varepsilon_u) = 55\text{MPa} \\ W(\varepsilon_u,\psi) = w(\varepsilon_u) = 98.9\text{MPa} \\ \mathcal{G} = W - \mathcal{W} = 43.9\text{MPa} \end{cases} \tag{146}$$

If we subsequently unload the material to a strain of value $\varepsilon = 1$, taking into account that during unloading–reloading ψ and $\mathcal{G}$ remain constant ($\dot{\psi} = 0$, $\mathcal{G} = 0$), we obtain that $\Delta W = \Delta\mathcal{W}$, and

$$\begin{cases} \sigma = \psi\sigma_m = \psi E_m\varepsilon = 27.5\text{MPa} \\ \mathcal{W}(\varepsilon,\psi) = \psi\mathcal{W}_m(\varepsilon) = \frac{1}{2}\psi E_m\varepsilon^2 = 13.75\text{MPa} \\ W(\varepsilon,\psi) = W(\varepsilon_u,\psi) - (\mathcal{W}(\varepsilon_u,\psi) - \mathcal{W}(\varepsilon),\psi) \\ \qquad\qquad = 57.65\text{MPa} \\ \mathcal{G} = W - \mathcal{W} = 43.9\text{MPa(no change)} \end{cases} \tag{147}$$

All these quantities can be verified in Fig. 8b.

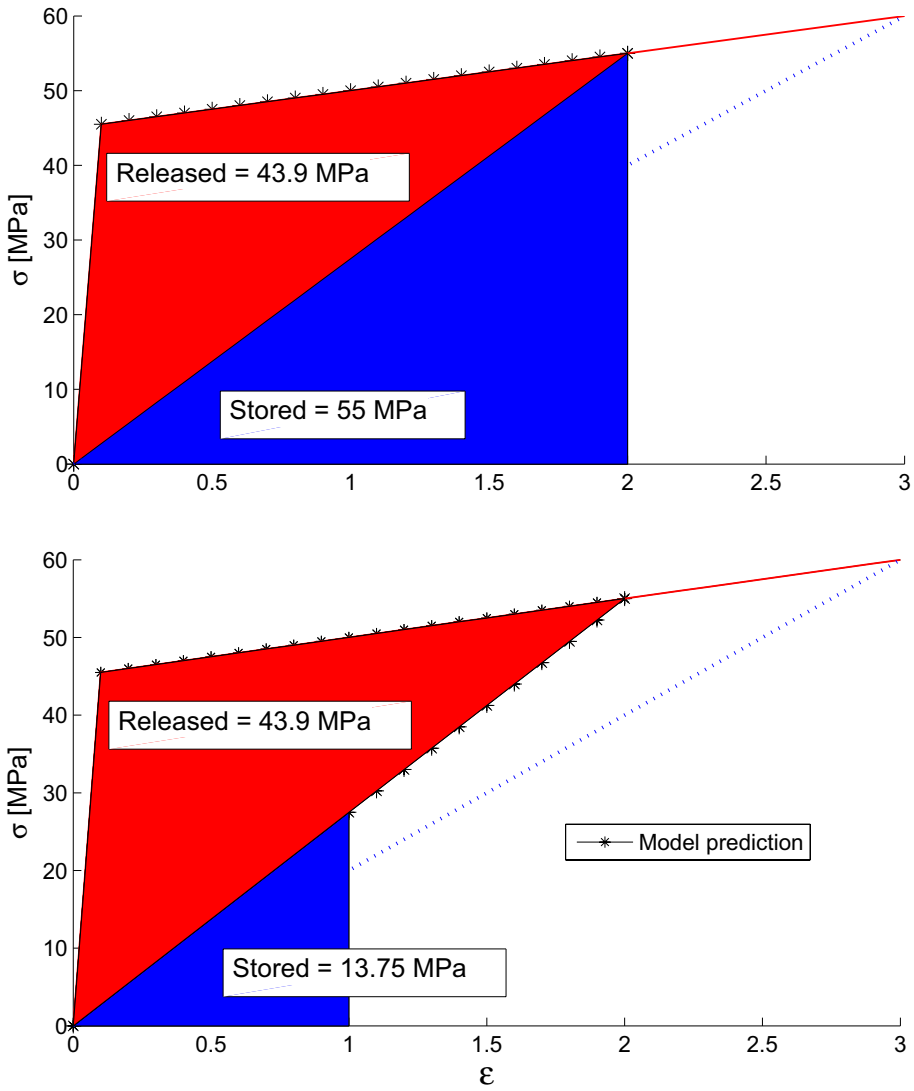

Fig. 8 Uniaxial test for a bilinear behaviour material. *Top* released and stored energies involved in the loading case. *Bottom* the same for the unloading case

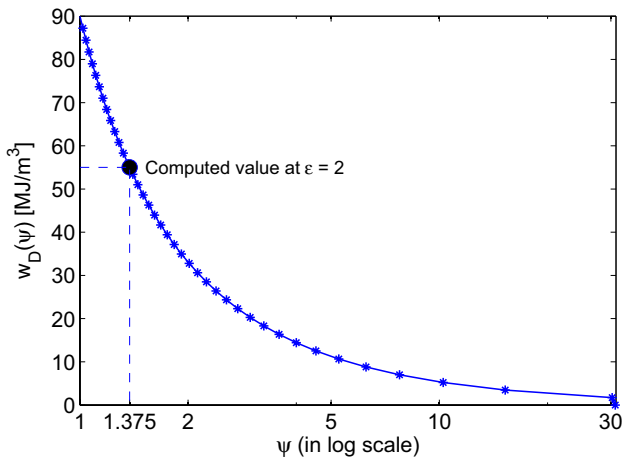

Fig. 9 Computed damage variable function against the proportionality parameter for the bilinear example

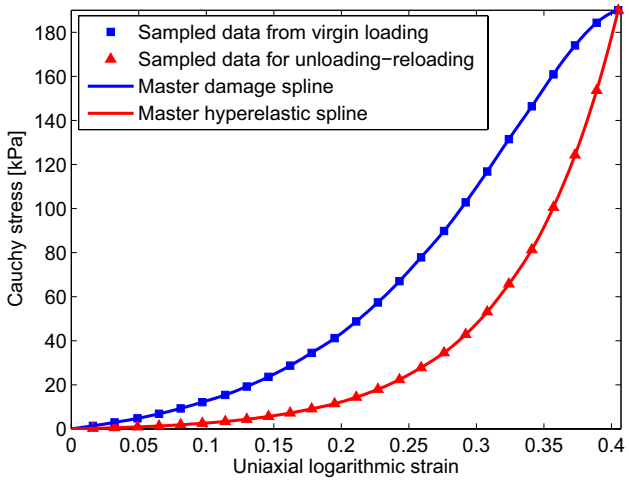

Fig. 10 Experimental data extracted from ref. [89] and initial uniform spline interpolation for the isotropic case

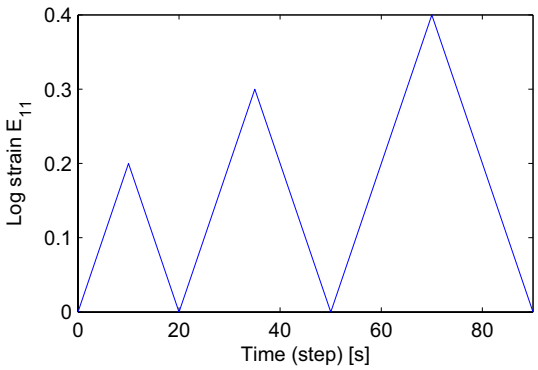

Fig. 11 Prescribed uniaxial strain history

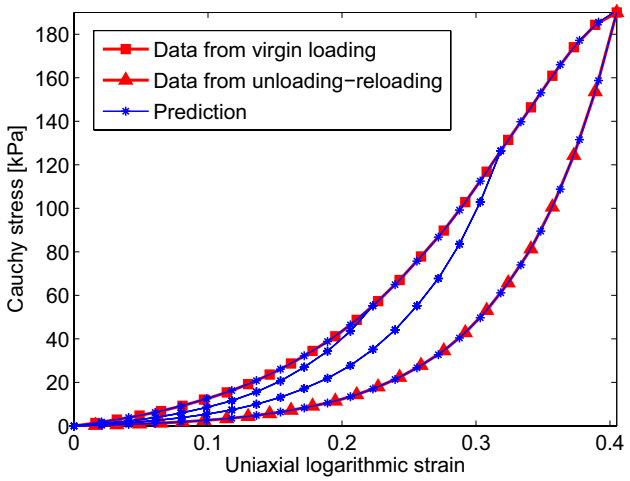

Fig. 12 Predictions for the uniaxial test versus uniaxial prescribed data

In Fig. 9 the damage variable versus the proportionality parameter $w_D(\psi)$ has been plotted, recall Eq. (20).

6.2 Isotropic Material

The aim of this example is to show the capabilities of the spline-based damage model for isotropic hyperelastic materials. The material data needed is an experimental virgin loading curve and a unloading–reloading curve which must be given up to the maximum value of strain that will be attained during the simulations. To show the applicability to soft biological tissues, we evaluate our model using tensile test data on intraluminal venous thrombus extracted from ref. [89]. Due to the absence of reported experimental data for the compression behavior, which is needed to properly define the material, we have assumed an antisymmetric stress distribution $\tilde{\sigma}_i(-\tilde{E}_i) = -\tilde{\sigma}_i(\tilde{E}_i)$. The experimental data used are shown in Fig. 10.

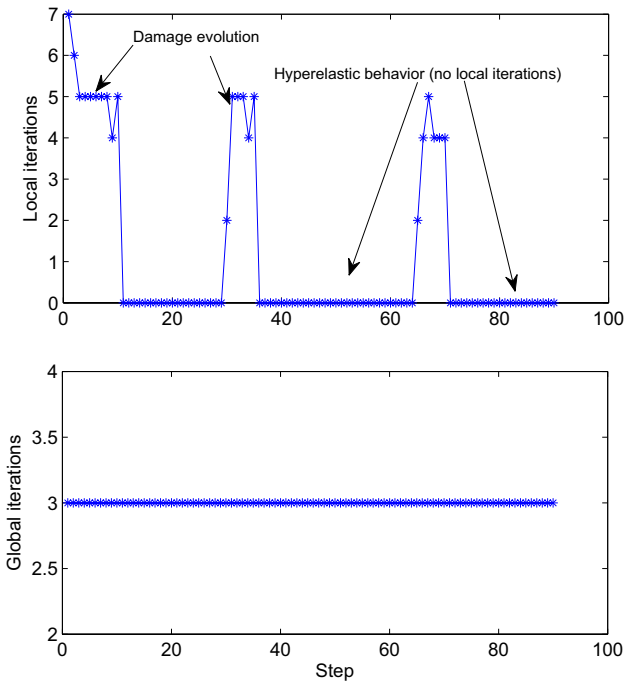

Fig. 13 Uniaxial test of an isotropic material. *Top* local iterations employed in the computation of ψ per global iteration. *Bottom* number of global iterations invested per step

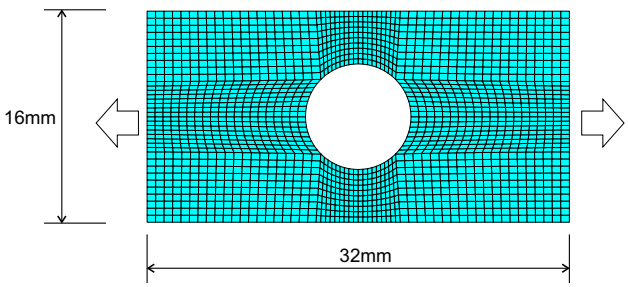

Fig. 14 *Rectangular plate with a concentric hole* reference configuration and finite element mesh

As a first simulation we have considered a tensile test with the prescribed uniaxial strain history E_{11} shown in Fig. 11, where due to incompressibility we have $E_2 = E_3 = -\frac{1}{2}E_1$. An initially undeformed block of $100 \times 100 \times 100$ is deformed longitudinally up to a dimension of 150. As it can be seen in Fig. 12, the predicted stress–strain data exactly mimic the prescribed data. Plain Newton algorithms (without line searches) have been employed both locally and globally. The number of local iterations employed in the computation of the energy multiplier parameter ψ, i.e. the number of iterations to fulfill the consistency condition of Eq. (90) up to a relative tolerance of 10^{-10}, are shown in Fig. 13a. It can be noticed that local iterations are necessary only during damage evolution. The

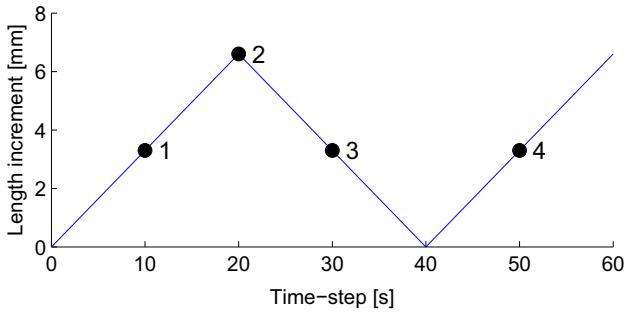

Fig. 15 Prescribed uniaxial strain for the uniaxial test performed on the isotropic rectangular plate. The *dots* represent the time-steps shown in the deformed meshes

number of these global equilibrium iterations invested per step are always three, as can be observed in the Fig. 13b. It is noted that there is no correlation between Fig. 13a, b, because the degree of non-linearity in both curves, master damage and master hyperelastic curves, is similar as can be observed in Fig. 10, so the number of global iterations is independent of whether damage is evolving or not.

As a second simulation in order to assess the applicability of the model to more complex situations and to show the efficiency of the constitutive tangent, a bidimensional plate with a concentric circular hole made of the same incompressible isotropic hyperelastic material is stretched under a plane strain condition in x-direction up to a total length of $l = 38.6$ mm. The initial dimensions are, length $l_0 = 32$ mm, height $h_0 = 16$ mm and inner radius $r_0 = 4$ mm. The geometry and finite element discretization of the undeformed plate are depicted in Fig. 14. This example has been used in a number of publications using different constitutive models [77, 80, 84, 85].

The deviatoric reponses of the master hyperelastic and master damaged curves of our procedure are described by isotropic spline-based WYPiWYG strain energy functions—cf. Ref. [77]. The volumetric penalty stored energy that we have used in the examples is the typical

$$\mathcal{U}(J) = \frac{1}{2}k(J-1)^2 \tag{148}$$

where J is the Jacobian determinant of the deformation, k is the bulk modulus (penalty parameter), which we took as $k = 10$ MPa. In order to avoid mesh-locking, fully integrated (3×3 Gauss integration) 9 / 3 u/p mixed finite elements are used, see [88]. For the incremental (global) analysis, a Newton-Raphson scheme, without line searches, is employed. The history of the imposed displacements via penalty method are shown in Fig. 15.

In Fig. 16, the deformed configuration of the plate and the distribution of the computed von Mises stress are depicted. In Fig. 17 we show the simulations performed

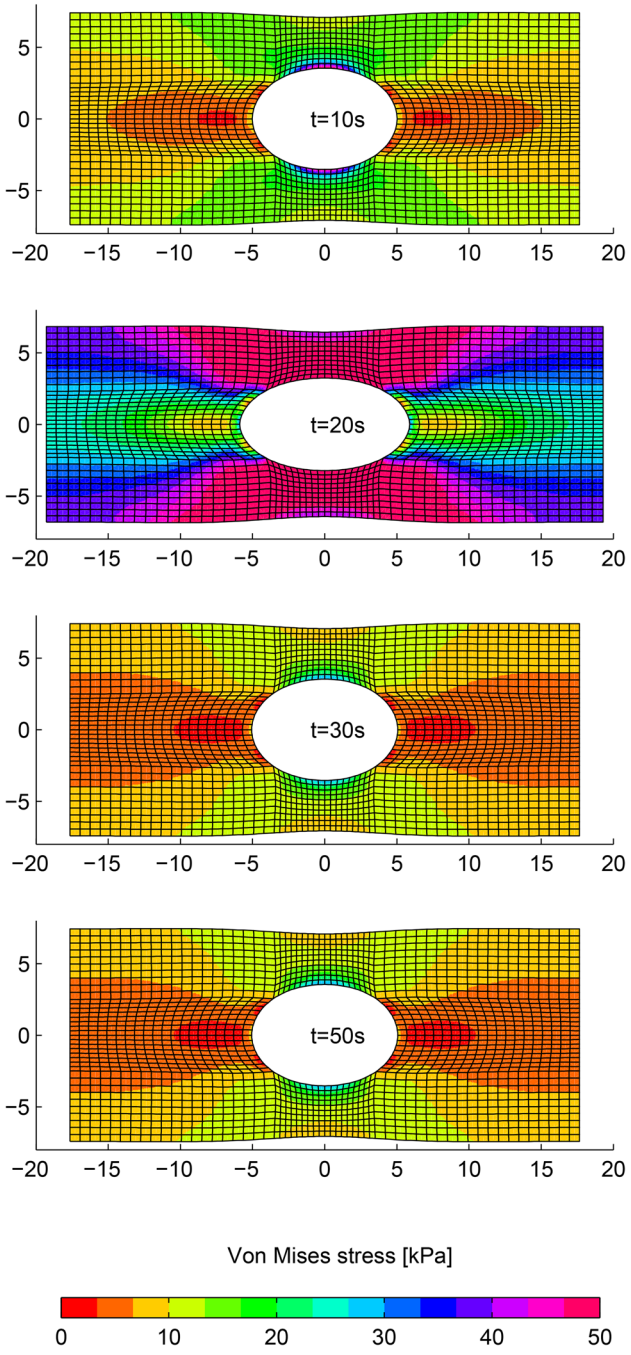

Fig. 16 Uniaxial tension of a *rectangular plate with a concentric circular hole* under a plain strain condition using the isotropic damage model: deformed configuration (maximum length = 38.6 mm) and distributions of von Mises stress at instants $t = 10$ s, $t = 20$ s, $t = 30$ s and $t = 50$ s. Note that for comparison, the color scale is the same for all plates. The maximum stress for $t = 20$ s is close to the maximum of $180kPa$ given in Fig. 12

using the master damage curve as if it were from a hyperelastic material without damage. Then, the differences between Figs. 16 and 17 are due to damage evolution.

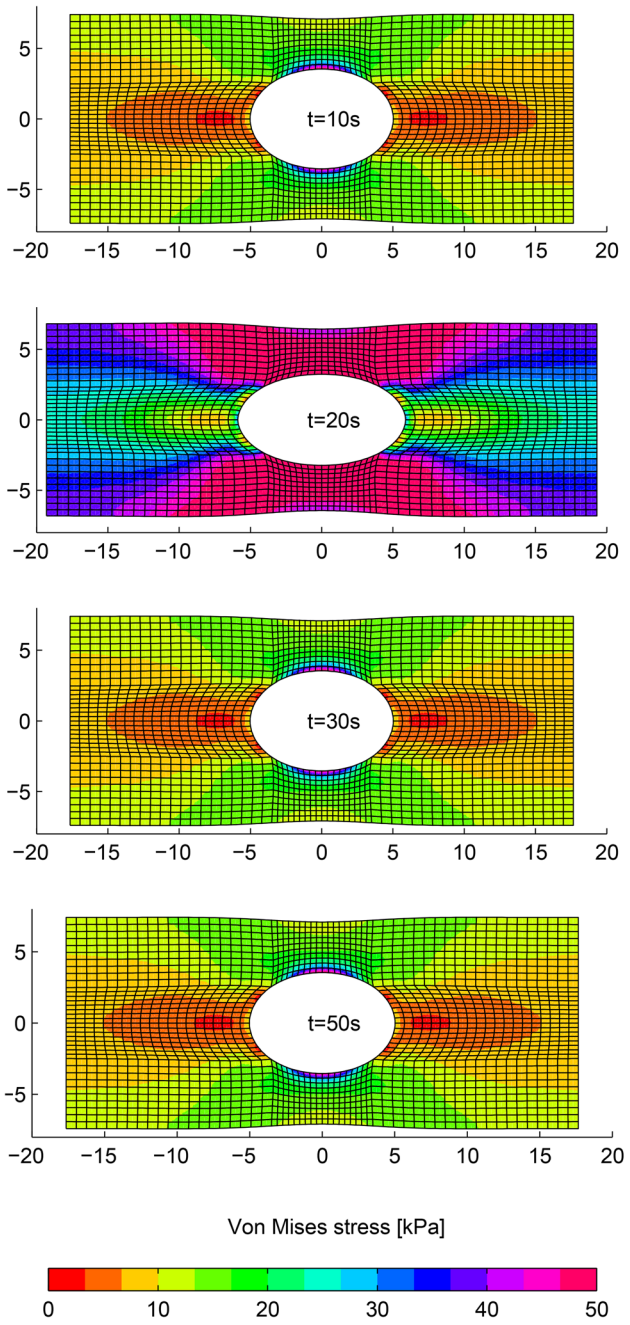

Fig. 17 Uniaxial tension of a rectangular plate with a concentric circular hole under a plain strain condition using the isotropic hyperelastic model: deformed configuration (maximum length = 38.6 mm) and distributions of von Mises stress at instants, $t = 10$ s, $t = 20$ s, $t = 30$ s and $t = 50$ s

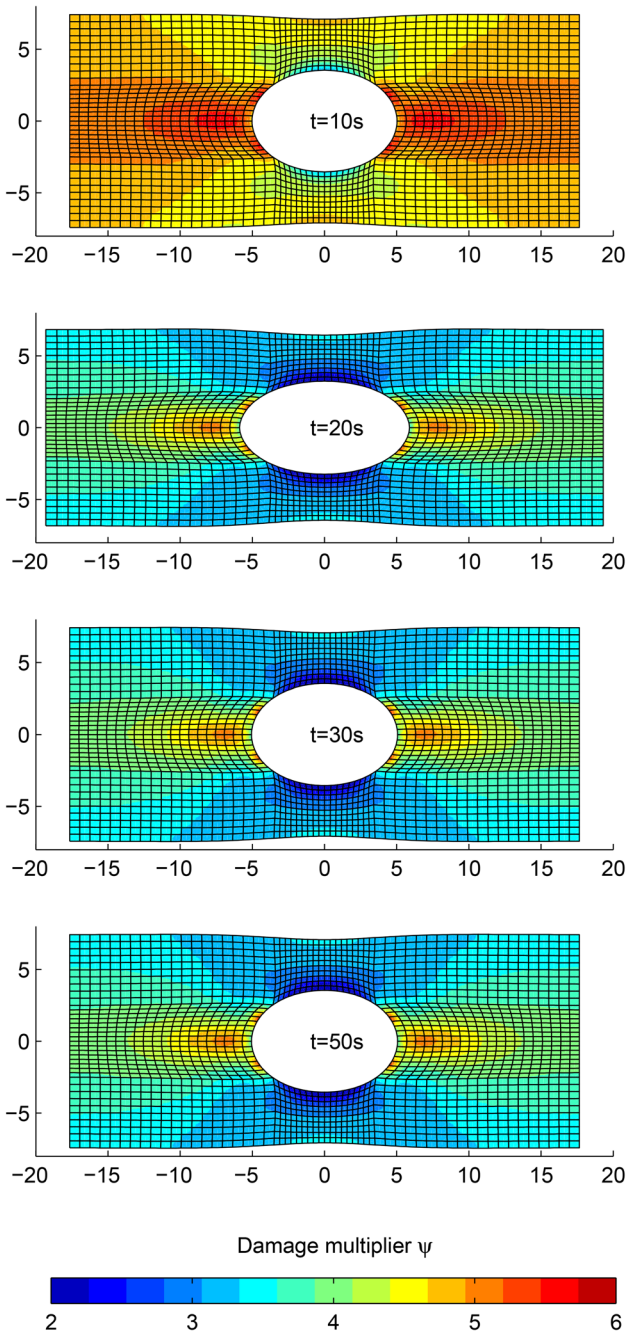

Fig. 18 Distributions of the isotropic damage variable ψ at instants $t = 10$ s, $t = 20$ s, $t = 30$ s and $t = 50$ s

In Fig. 18, the distribution of the isotropic damage variable ψ is represented. It can be observed that the locations with the highest concentration of stresses are the most damaged ones, i.e. the value of the damage variable tends to the reference value ($\psi_D = 1$). It can also be noticed that even if the material is unloaded, once the material is damaged, this phenomenon is irreversible, so the material does not heal and the parameter ψ remains constant upon unloading and reloading.

As it can be observed in Table 1, typically four of global equilibrium iterations are invested to reach a relative unequilibrated forces tolerance of 10^{-8}, and there is no relevant penalty in the global iterations because of damage evolution, i.e. the number of global iterations employed

Table 1 Convergence rates of the equilibrium iterations for the example of the plate with a hole. Isotropic model

Relative global convergence rates. Isotropic plate		
Step (Iter)	Force	Energy
10(1)	1.00E+00	1.00E+00
10(2)	5.92E−04	1.30E−06
10(3)	1.82E−06	9.65E−13
10(4)	4.68E−10	3.51E−18
20(1)	1.00E+00	1.00E+00
20(2)	5.89E−04	1.30E−06
20(3)	1.00E−06	5.91E−13
20(4)	7.98E−10	5.57E−18
30(1)	1.00E+00	1.00E+00
30(2)	5.58E−04	1.27E−06
30(3)	1.13E−06	6.79E−13
30(4)	9.30E−12	6.44E−24
50(1)	1.00E+00	1.00E+00
50(2)	5.84E−04	1.30E−06
50(3)	1.20E−06	4.12E−13
50(4)	1.44E−11	2.34E−23

are mainly a consequence of the nonlinear hyperelastic behavior.

6.3 Orthotropic Material

We show now some illustrative examples using modified uniaxial data to represent anisotropy. To our knowledge there is no work in the literature containing all the experimental data needed to fully define the orthotropic non-linear damage behavior, so assumed test data have been employed in this example, shown in Fig. 19. For compression, we have also assumed an antisymmetric stress distribution $\tilde{\sigma}_i(-\tilde{E}_i) = -\tilde{\sigma}_i(\tilde{E}_i)$. It should be noted that if the mentioned complete set of experimental data were available, our procedure would be able to reproduce "exactly" the behavior of all the curves simultaneously, quite regardless of the shape thereof, and that in the absence of a complete set, some of them can be assumed without affecting the goodness of the predictions for the other ones.

As a first demonstrative example, we have performed three uniaxial tests in the three principal material directions $\boldsymbol{a}_1$, $\boldsymbol{a}_2$ and $\boldsymbol{a}_3$, respectively, loading and unloading several times up to the maximum value of strain for which the experimental master damage curve is defined for each of the preferred directions of the material. In this case we have used a new specimen for each test. As it can be observed in Fig. 20, the predicted stress–strain data exactly simulate the prescribed experimental data for primary loading but not for unloading ones as we explain below. Then we have performed again three tests in the principal material directions but this time the tests have been performed on the same specimen, successively (just one new specimen is needed). As expected, the results in this case, shown in Fig. 21, are different from the previous case and do not reproduce the primary loading experimental data in the last two tests since after loading in one direction and unloading, the material is irreversibly damaged. Recall that axial components are coupled by the incompressibility condition and the isotropic contribution, when

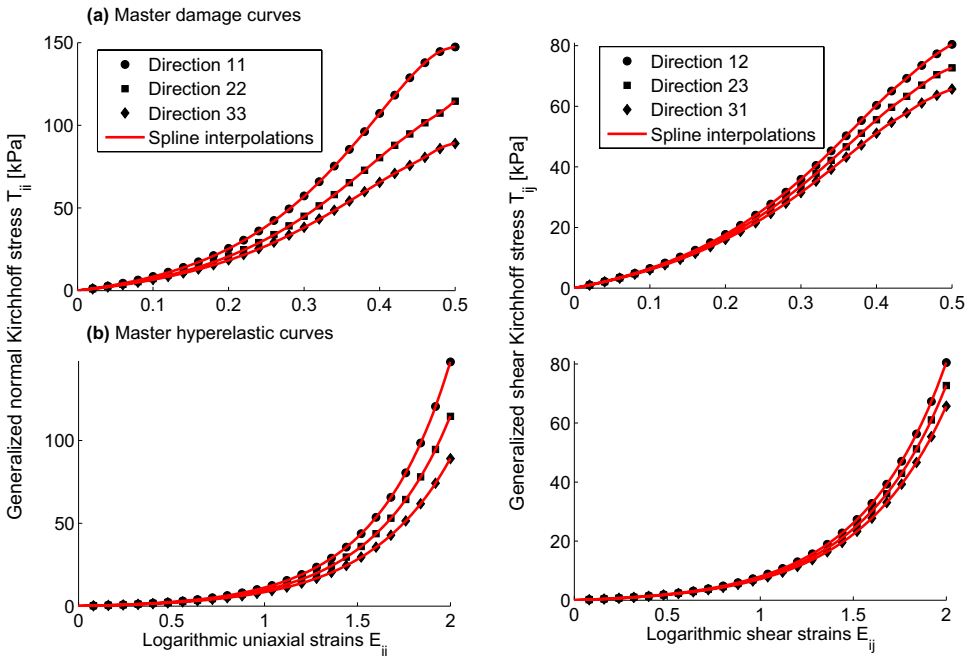

Fig. 19 Experimental data and initial uniform spline interpolation. **a** Original stress–strain data and spline fit for the master damage curves corresponding to the uniaxial and shear tests. **b** Data for the master hyperelastic curves

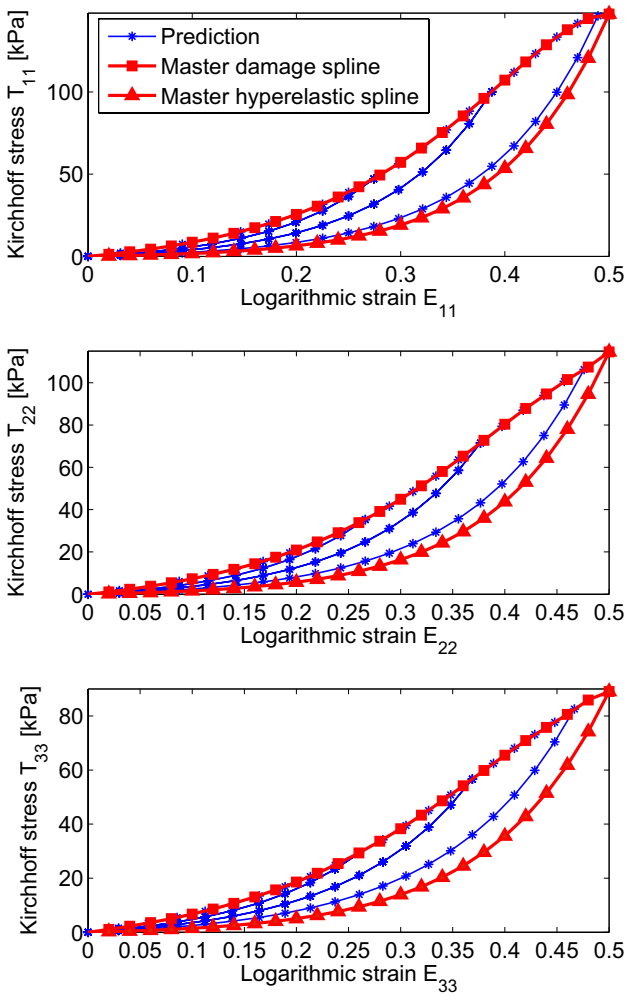

Fig. 20 Predictions for the three uniaxial tests performed in the three preferred directions $\{\boldsymbol{a}_1, \boldsymbol{a}_2, \boldsymbol{a}_3\}$ respectively, on different samples

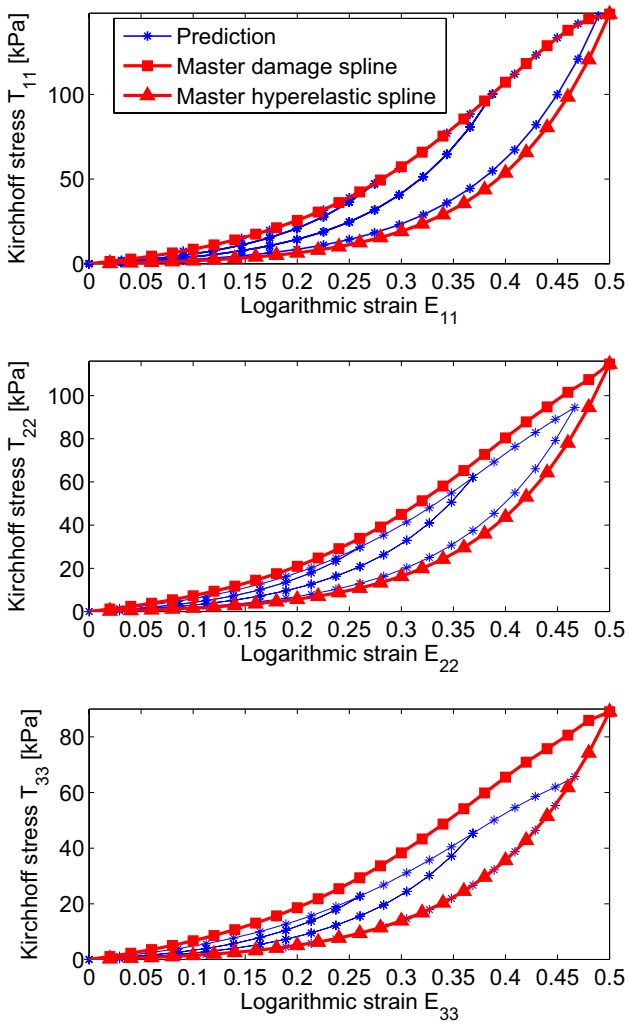

Fig. 21 Predictions for the three uniaxial tests performed in the three preferred directions $\{\boldsymbol{a}_1, \boldsymbol{a}_2, \boldsymbol{a}_3\}$ respectively, on the same sample

considered. However, as expected, we can see that in the third test (performed in the preferred direction $\boldsymbol{a}_3$), during unloading the model captures accurately the experimental data corresponding to the master hyperelastic curve in that direction, as the variable of damage has reached the maximum in all three preferred directions. The master hyperelastic curve is only captured when the material has been damaged to the maximum in the three preferred directions. Therefore, previously, in the tests carried out on different specimens, the master hyperelastic curves were not reproduced as it would be expected. Of course, other possible definitions for the master hyperelastic curve are possible, and hence that curve will captured when the deformation procedure corresponds to such definition. Note that inherent to the definition of the master hyperelastic curve is the procedure needed to reach such deformation/damage state.

As a second anisotropic simulation we have prescribed a pure shear state, again loading and unloading several times

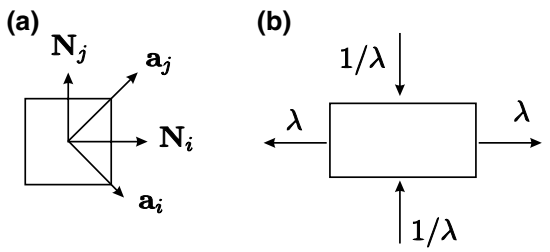

Fig. 22 Pure shear test in the plane $ij = 12$. **a** Representation of the reference configuration in principal strain basis $\{\boldsymbol{N}_i, \boldsymbol{N}_j, \boldsymbol{N}_k\}$ with $(i \neq j \neq k)$ and $\boldsymbol{a}_i$ and $\boldsymbol{a}_j$ define the orientation of the material preferred directions. **b** Kinematics of deformation in the biaxial test and its associated principal stretches

to observe the Mullins effect. Some specific biaxial tests (e.g. plane strip tensile tests) carried out over orthotropic materials lead to pure shear state for logarithmic strains in specific

reference systems, see ref. [87]. According to this, we have imposed the following deformation gradient in the basis of principal stretches $\boldsymbol{N} = \{\boldsymbol{N}_1, \boldsymbol{N}_2, \boldsymbol{N}_3\}$—see Fig. 22a and take $i, j, k = 1, 2, 3$

$$ {}^{t}_{0}\boldsymbol{X} = \begin{bmatrix} \lambda & 0 & 0 \\ 0 & 1/\lambda & 0 \\ 0 & 0 & 1 \end{bmatrix}_{\boldsymbol{N}} \tag{149} $$

As an example, the material is loaded in tension in direction $\boldsymbol{N}_1$ and in compression in direction $\boldsymbol{N}_2$ to attain the prescribed stretches. We consider a plane stress state, i.e. the direction $\boldsymbol{N}_3$ can be considered as free of tractions. Accordingly, the Hencky strain tensor components are $E_1 = \ln(\lambda)$, $E_2 = \ln(1/\lambda) = -E_1$, $E_3 = 0$. Note that the imposed deformations are isochoric. The orientation of the reference configuration and the orientation of the material preferred directions (clockwise 45° with respect to $\boldsymbol{N}_1$) are shown in Fig. 22 a. The deformation imposed is depicted in Fig. 22b. The projection of the corresponding Hencky strain tensor $\boldsymbol{E}$ into the basis of the material preferred directions $\boldsymbol{A} = \{\boldsymbol{a}_1, \boldsymbol{a}_2, \boldsymbol{a}_3\}$ furnishes the pure shear state

$$ \boldsymbol{E} = \begin{bmatrix} 0 & E_1 & 0 \\ E_1 & 0 & 0 \\ 0 & 0 & 0 \end{bmatrix}_{\boldsymbol{A}} \tag{150} $$

Therefore, the tensor $\boldsymbol{T}$ is simply

$$ \boldsymbol{T} = \begin{bmatrix} 0 & \omega'_{12}(E) & 0 \\ \omega'_{12}(E) & 0 & 0 \\ 0 & 0 & 0 \end{bmatrix}_{\boldsymbol{A}} \tag{151} $$

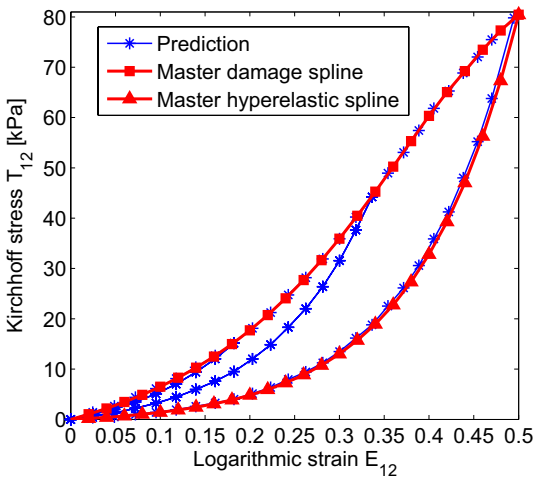

Fig. 23 Pure shear test prediction

resulting a state of pure shear also in stresses, which implies that for this particular test, principal directions of stresses and strains are coincident and thus $\boldsymbol{E}$ and $\boldsymbol{T}$ commute as well as $\boldsymbol{T}$ is completely coincident with $\boldsymbol{\sigma}$, see [87]. Then, the Cauchy stress tensor expressed in the basis of principal stretches is

$$ \boldsymbol{\sigma} = \boldsymbol{T} = \begin{bmatrix} \omega'_{12}(E) & 0 & 0 \\ 0 & -\omega'_{12}(E) & 0 \\ 0 & 0 & 0 \end{bmatrix}_{\boldsymbol{N}} \tag{152} $$

The results are shown in Fig. 23. Once again it can be seen as the model accurately reproduces the experimental data for the shear stress T_{12}.

In order to illustrate the finite element simulation capabilities of the presented orthotropic damage model, several numerical examples are performed over the bidimensional plate with a concentric circular hole made of a nearly incompressible orthotropic hyperelastic material in which the preferred material axes are not aligned with the test axes. As in the isotropic example, the plate is loaded about the x-axis in this case up to a maximum length of 40 mm. The volumetric contribution $\mathcal{U}$ to $\mathcal{W}$ that we have used in the examples is given in Eq. (148), in this particular case a value of k= 30 MPa has been selected to numerically enforce incompressibility. We have used the same mesh and element types as in the isotropic example. For the incremental (global) analysis, a Newton–Raphson scheme, without line searches, is also employed.

In order to appreciate the effects of anisotropy, we have oriented the principal material direction $\alpha = 30°$ counterclockwise away from the horizontal direction. The deformed shapes and von Mises stresses for different relevant steps are shown in Fig. 24. The results of an equivalent hyperelastic model, not shown, are identical to those given in Fig. 24 for $t = 10$ s and $t = 20$ s, whereas the results for $t = 30$ s and $t = 50$ s are identical to those of $t = 10$ s (in accordance to the hyperelastic nature). In the case of the orthotropic damage model, it is seen that the unloading and the reloading coincide for the same deformation, below the maximum value reached before unloading.

The distributions of the damage variables ψ_{11} and ψ_{12} for the different selected times are shown in Figs. 25 and 26, where it can be seen that the most damaged locations are those that sustain more stress and that once a value of damage is reached, the material does not heal even if the specimen is completely unloaded. Furthermore, the damage patterns for the different ψ variables are in accordance which what would be qualitatively expected for each deformation mode.

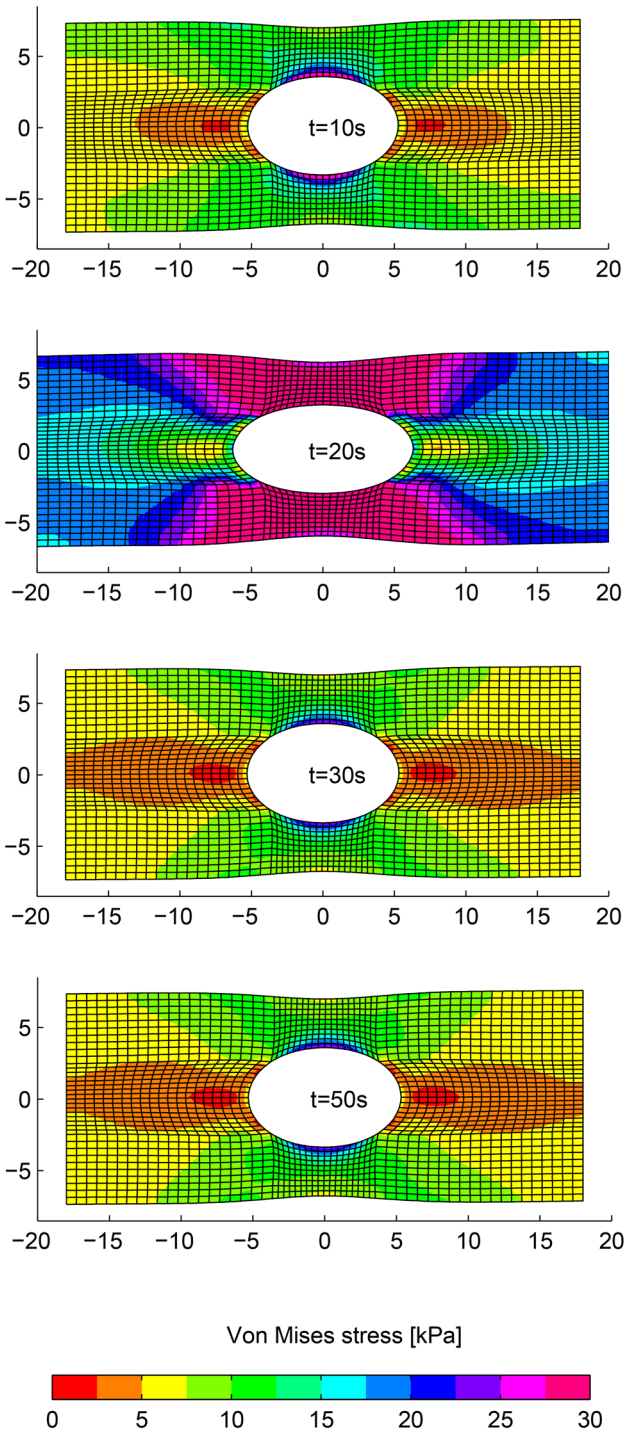

Fig. 24 Uniaxial tension of a *rectangular plate with a concentric circular hole* under a plain strain condition using the orthotropic hyperelastic damage model: deformed configurations (maximum length = 40 mm) and distributions of von Mises stress (kPa) at instants $t = 10$ s, $t = 20$ s, $t = 30$ s and $t = 50$ s

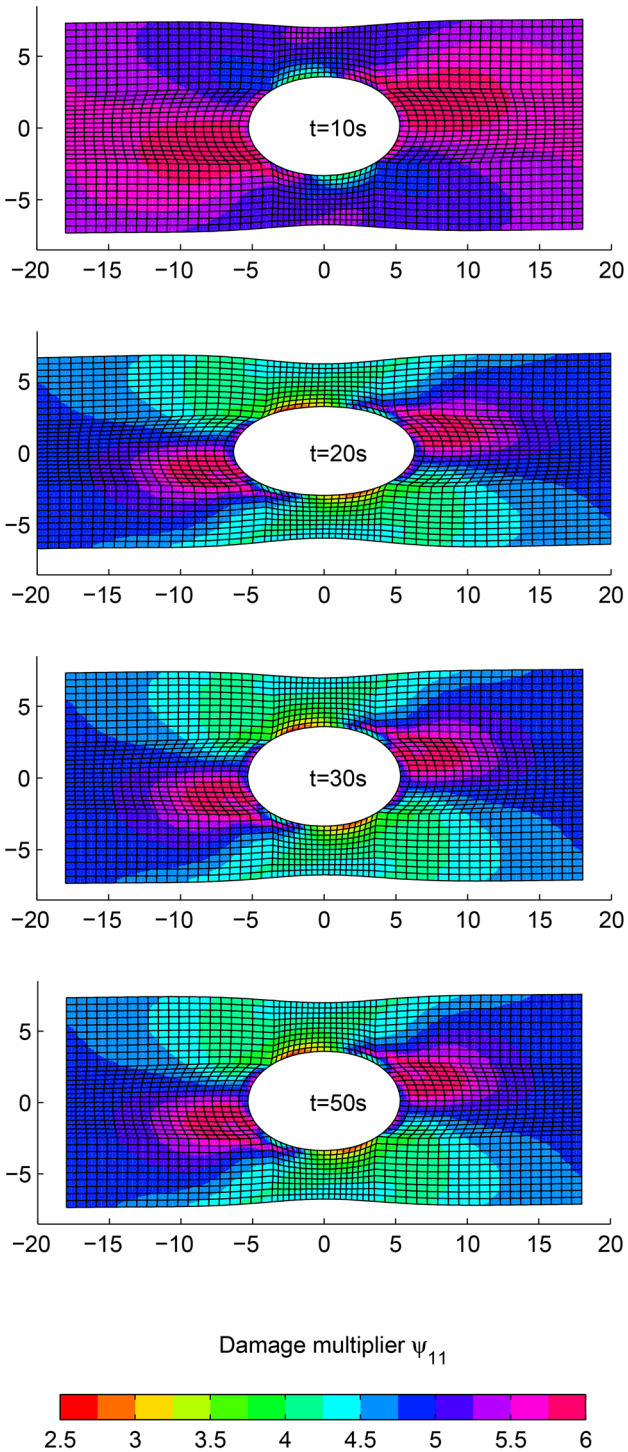

Fig. 25 Distributions of the damage variable ψ_{11} associated with the preferred direction $\boldsymbol{a}_1$ for $t = 10$ s, $t = 20$ s, $t = 30$ s and $t = 50$ s

Table 2 shows that quadratic force and energy rates of convergence are obtained in typical steps of primary loading (steps 10 and 20), unloading (step 30) and reloading (step 50). Execution times for the damage model are in the same order of the hyperelastic model because, although not needed, even if local iterations are used for the isotropic component, they represent a small amount of the total computation time.

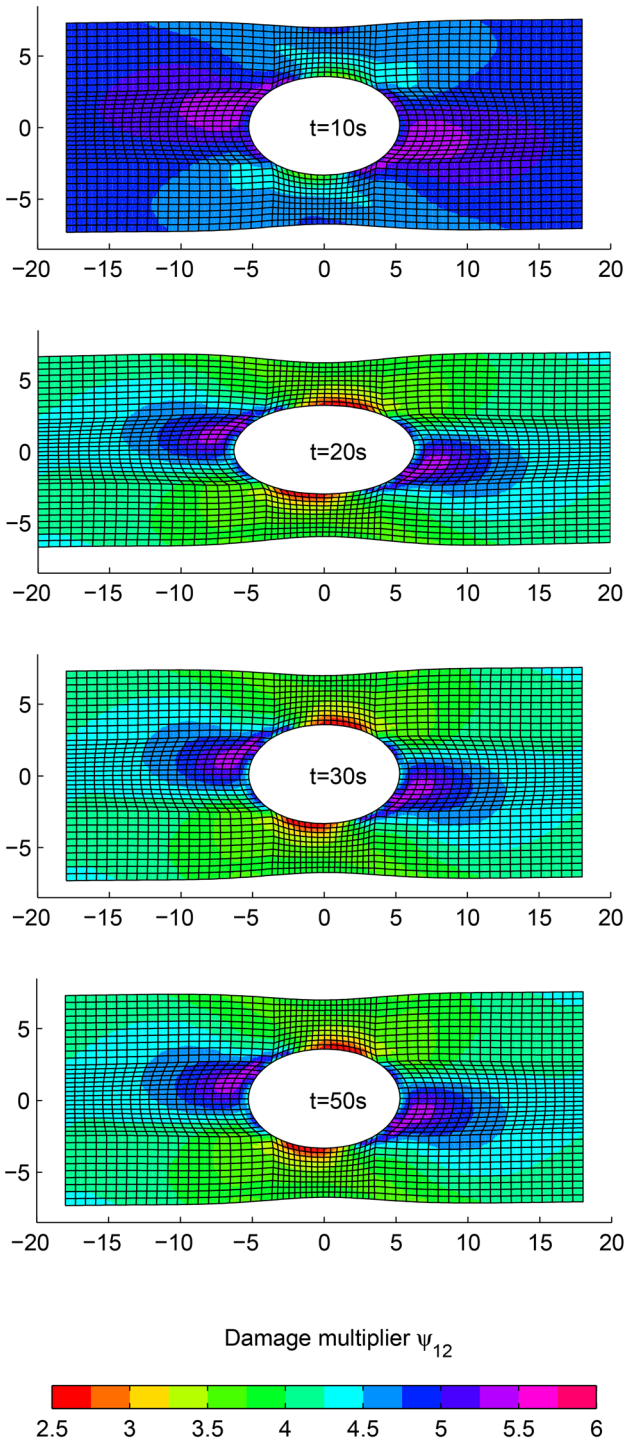

Fig. 26 Distributions of the damage variable ψ_{12} associated with the shearing component in the preferred directions $\boldsymbol{a}_1 - \boldsymbol{a}_2$ for $t = 10$ s, $t = 20$ s, $t = 30$ s and $t = 50$ s

7 Conclusions

In this work we have developed a WYPiWYG formulation for damage mechanics in isotropic and anisotropic materials. We have motivated the formulation in detail using a one-dimensional infinitesimal example in which the ideas are easily exposed. It is seen that two potentials may be employed, resulting respectively in frameworks similar to those of Continuum Damage Mechanics and Pseudoelasticity. However, following the ideas of the WYPiWYG approach, no analytical functions are imposed in the hyperelastic and damage evolution constitutive equations. Instead, the information is extracted from a complete set of experimental tests, solving numerically the corresponding differential equations. The procedure is purely phenomenological and, hence, valid for polymers and biological tissues. The formulation may be split into an isotropic contribution (for example from an isotropic matrix) and an orthotropic one (for example from reinforcements). The modelling procedure is capable of capturing simultaneously the behavior observed in six independent experiments showing Mullins effect.

We have developed the corresponding algorithmic formulation, which computational time is of the same order than that of hyperelastic models. Finite element examples for both isotropic and anisotropic behavior show that the global equilibrium iterations are very efficient, because the convergence rates are equivalent to those obtained using a hyperelastic model without damage.

Table 2 Relative convergence rates during equilibrium iterations in the example of the plate with a hole. Anisotropic damage

Relative global convergence rates. Anisotropic plate		
Step (Iter)	Force	Energy
10(1)	1.00E+00	1.00E+00
10(2)	8.83E−04	2.51E−06
10(3)	4.14E−07	1.83E−13
20(1)	1.00E+00	1.00E+00
20(2)	8.56E−04	2.23E−06
20(3)	4.51E−07	2.92E−14
30(1)	1.00E+00	1.00E+00
30(2)	8.19E−04	2.43E−06
30(3)	3.98E−07	1.68E−14
50(1)	1.00E+00	1.00E+00
50(2)	8.70E−04	2.48E−06
50(3)	4.92E−07	2.86E−14

Acknowledgements Partial financial support for this work has been given by grant DPI2015-69801-R from the Dirección General de Proyectos de Investigación of the Ministerio de Economía y Competitividad of Spain. FJM acknowledges the support of the Department of Mechanical and Aerospace Engineering of University of Florida during the sabbatical period in which part of this work was done, and Ministerio de Educación, Cultura y Deporte of Spain for the financial support for that stay under Grant PRX15/00065.

Compliance with Ethical Standards

Conflicts of interest The authors declare that there are no conflicts of interest.

References

1. Treloar LRG (1975) The physics of rubber elasticity. Oxford University Press, Oxford
2. Ogden RW (1997) Non-linear elastic deformations. Courier Corporation, New York
3. Bergstrom JS (2015) Mechanics of solid polymers: theory and computational modeling. Elsevier, Amsterdam
4. Fung YC (1993) Biomechanics: mechanical properties of living tissues. Springer, New York
5. Humphrey JD (2002) Cardiovascular solid mechanics: cells, tissues, and organs. Springer, New York
6. Holzapfel GA (2000) Nonlinear solid mechanics, vol 24, Wiley, Chichester
7. Bonet J, Wood RD (1997) Nonlinear continuum mechanics for finite element analysis. Cambridge University Press, Cambridge
8. Ogden RW (1973) Large deformation isotropic elasticity-on the correlation of theory and experiment for incompressible rubberlike solids. Rubber Chem Technol 46(2):398–416
9. Fung YC, Fronek K, Patitucci P (1979) Pseudoelasticity of arteries and the choice of its mathematical expression. Am J Physiol Heart Circ Physiol 237(5):H620–H631
10. Itskov M, Ehret AE (2009) A universal model for the elastic, inelastic and active behaviour of soft biological tissues. GAMM-Mitteilungen 32(2):221–236
11. Ehret AE, Itskov M (2009) Modeling of anisotropic softening phenomena: application to soft biological tissues. Int J Plast 25(5):901–919
12. Itskov M, Aksel N (2004) A class of orthotropic and transversely isotropic hyperelastic constitutive models based on a polyconvex strain energy function. Int J Solids and Struct 41(14):3833–3848
13. Lanir Y (1983) Constitutive equations for fibrous connective tissues. J Biomech 16(1):1–12
14. Humphrey JD, Yin FC (1987) A new constitutive formulation for characterizing the mechanical behavior of soft tissues. Biophys J 52(4):563–570
15. Holzapfel GA, Gasser TC, Ogden RW (2000) A new constitutive framework for arterial wall mechanics and a comparative study of material models. J Elast Phys Sci Solids 61(1–3):1–48
16. Gasser TC, Ogden RW, Holzapfel GA (2006) Hyperelastic modelling of arterial layers with distributed collagen fibre orientations. J R Soc Interface 3(6):15–35
17. Ogden RW, Saccomandi G, Sgura I (2004) Fitting hyperelastic models to experimental data. Comput Mech 34(6):484–502
18. Groves RB, Coulman SA, Birchall JC, Evans SL (2013) An anisotropic, hyperelastic model for skin: experimental measurements, finite element modelling and identification of parameters for human and murine skin. J Mech Behav Biomed Mater 18:167–180
19. Kvistedal YA, Nielsen PMF (2009) Estimating material parameters of human skin in vivo. Biomech Model Mechanobiol 8(1):1–8
20. Latorre M, Montáns FJ (2015) Material-symmetries congruency in transversely isotropic and orthotropic hyperelastic materials. Eur J Mech A Solids 53:99–106
21. Latorre M, Montáns FJ (2016) On the tension-compression switch of the Gasser–Ogden–Holzapfel model: analysis and a new pre-integrated proposal. J Mech Behav Biomed Mater 57:175–189
22. Latorre M, Romero X, Montáns FJ (2016) The relevance of transverse deformation effects in modeling soft biological tissues. Int J Solids Struct 99:57–70
23. Skacel P, Bursa J (2016) Poisson's ratio of arterial wall-Inconsistency of constitutive models with experimental data. J Mech Behav Biomed Mater 54:316–327
24. Latorre M, De Rosa E, Montáns FJ (2017) Understanding the need of the compression branch to characterize hyperelastic materials. Int J Non-Linear Mech 89:14–24
25. Murphy JG (2013) Transversely isotropic biological, soft tissue must be modelled using both anisotropic invariants. Eur J Mech A Solids 42:90–96
26. Murphy JG (2014) Evolution of anisotropy in soft tissue. Proceedings of the Royal Society A (Vol 470, no. 2161, p 20130548)
27. Mullins L (1948) Effect of stretching on the properties of rubber. Rubber Chem Technol 21(2):281–300
28. Mullins L (1969) Softening of rubber by deformation. Rubber Chem Technol 42(1):339–362
29. Blanchard AF, Parkinson D (1952) Breakage of carbon-rubber networks by applied stress. Ind Eng Chem 44(4):799–812
30. Bueche F (1960) Molecular basis for the Mullins effect. J Appl Polym Sci 4(10):107–114
31. Houwink R (1956) Slipping of molecules during the deformation of reinforced rubber. Rubber Chem Technol 29(3):888–893
32. Hanson DE, Hawley M, Houlton R, Chitanvis K, Rae P, Orler EB, Wrobleski DA (2005) Stress softening experiments in silica-filled polydimethylsiloxane provide insight into a mechanism for the Mullins effect. Polymer 46(24):10989–10995
33. Kraus G, Childers CW, Rollmann KW (1966) Stress softening in carbon black reinforced vulcanizates. Strain rate and temperature effects. Rubber Chem Technol 39(5):1530–1543
34. Lion A (1996) A constitutive model for carbon black filled rubber: experimental investigations and mathematical representation. Continuum Mech Thermodyn 8(3):153–169
35. Diani J, Fayolle B, Gilormini P (2009) A review on the Mullins effect. Eur Polym J 45(3):601–612
36. Cribb AM, Scott JE (1995) Tendon response to tensile stress: an ultrastructural investigation of collagen: proteoglycan interactions in stressed tendon. J Anat 187(Pt 2):423
37. Scott JE (2003) Elasticity in extracellular matrix 'shape modules' of tendon, cartilage, etc. A sliding proteoglycan-filament model. J Physiol 553(2):335–343
38. Tang Y, Ballarini R, Buehler MJ, Eppell SJ (2010) Deformation micromechanisms of collagen fibrils under uniaxial tension. J R Soc Interface 7(46):839–850
39. Shen ZL, Dodge MR, Kahn H, Ballarini R, Eppell SJ (2010) In vitro fracture testing of submicron diameter collagen fibril specimens. Biophys J 99(6):1986–1995
40. Szczesny SE, Elliott DM (2014) Interfibrillar shear stress is the loading mechanism of collagen fibrils in tendon. Acta Biomater 10(6):2582–2590
41. Miñano M, Montáns FJ (2014) Engineering damage mechanics review. Civil Comp Press, Stirling
42. Simo JC (1987) On a fully three-dimensional finite-strain viscoelastic damage model: formulation and computational aspects. Comput Methods Appl Mech Eng 60(2):153–173
43. Govindjee S, Simo J (1991) A micro-mechanically based continuum damage model for carbon black-filled rubbers incorporating Mullins' effect. J Mech Phys Solids 39(1):87–112
44. Miehe C (1995) Discontinuous and continuous damage evolution in Ogden-type large-strain elastic materials. Eur J Mech A Solids 14(5):697–720

45. Calvo B, Peña E, Martínez MA, Doblaré M (2007) An uncoupled directional damage model for fibred biological soft tissues. Formulation and computational aspects. Int J Numer Meth Eng 69(10):2036–2057
46. Peña E (2014) Computational aspects of the numerical modelling of softening, damage and permanent set in soft biological tissues. Comput Struct 130:57–72
47. Peña E (2011) A rate dependent directional damage model for fibred materials: application to soft biological tissues. Comput Mech 48(4):407–420
48. Peña E, Doblaré M (2009) An anisotropic pseudo-elastic approach for modelling Mullins effect in fibrous biological materials. Mech Res Commun 36(7):784–790
49. Peña E, Peña JA, Doblaré M (2009) On the Mullins effect and hysteresis of fibered biological materials: a comparison between continuous and discontinuous damage models. Int J Solids Struct 46(7):1727–1735
50. Balzani D, Schmidt T (2015) Comparative analysis of damage functions for soft tissues: properties at damage initialization. Math Mech Solids 20(4):480–492
51. Martins P, Peña E, Jorge RN, Santos A, Santos L, Mascarenhas T, Calvo B (2012) Mechanical characterization and constitutive modelling of the damage process in rectus sheath. J Mech Behav Biomed Mater 8:111–122
52. Simo JC, Oliver J, Armero F (1993) An analysis of strong discontinuities induced by strain-softening in rate-independent inelastic solids. Comput Mech 12(5):277–296
53. Comellas E, Bellomo FJ, Oller S (2016) A generalized finite-strain damage model for quasi-incompressible hyperelasticity using hybrid formulation. Int J Numer Methods Eng 105(10):781–800
54. Sáez P, Alastrué V, Peña E, Doblaré M, Martínez MA (2012) Anisotropic microsphere-based approach to damage in soft fibered tissue. Biomechan Model Mechanobiol 11(5):595–608
55. Miehe C, Göktepe S, Lulei F (2004) A micro-macro approach to rubber-like materials–Part I: the non-affine micro-sphere model of rubber elasticity. J Mechan Phys Solids 52(11):2617–2660
56. Miehe C, Göktepe S (2005) A micro-macro approach to rubber-like materials. Part II: the micro-sphere model of finite rubber viscoelasticity. J Mechan Phys Solids 53(10):2231–2258
57. Göktepe S, Miehe C (2005) A micro-macro approach to rubber-like materials. Part III: the micro-sphere model of anisotropic Mullins-type damage. J Mech Phys Solids 53(10):2259–2283
58. Caner FC, Carol I (2006) Microplane constitutive model and computational framework for blood vessel tissue. J Biomechan Eng 128(3):419–427
59. Alastrué V, Sáez P, Martínez MA, Doblaré M (2010) On the use of the Bingham statistical distribution in microsphere-based constitutive models for arterial tissue. Mechan Res Commun 37(8):700–706
60. Famaey N, Vander Sloten J, Kuhl E (2013) A three-constituent damage model for arterial clamping in computer-assisted surgery. Biomechan Model Mechanobiol 12(1):123–136
61. Balzani D, Neff P, Schröder J, Holzapfel GA (2006) A polyconvex framework for soft biological tissues. Adjustment to experimental data. Int J Solids Struct 43(20):6052–6070
62. Volokh KY (2008) Prediction of arterial failure based on a microstructural bi-layer fiber-matrix model with softening. J Biomechan 41(2):447–453
63. Volokh KY (2011) Modeling failure of soft anisotropic materials with application to arteries. J Mechan Behav Biomed Mater 4(8):1582–1594
64. Rebouah M, Chagnon G (2014) Permanent set and stress-softening constitutive equation applied to rubber-like materials and soft tissues. Acta Mechan 225(6):1685–1698
65. Schmidt T, Balzani D, Holzapfel GA (2014) Statistical approach for a continuum description of damage evolution in soft collagenous tissues. Comput Methods Appl Mechan Eng 278:41–61
66. Blanco S, Polindara CA, Goicolea JM (2015) A regularised continuum damage model based on the mesoscopic scale for soft tissue. Int J Solids Struct 58:20–33
67. Balzani D, Ortiz M (2012) Relaxed incremental variational formulation for damage at large strains with application to fiber-reinforced materials and materials with truss-like microstructures. Int J Numer Methods Eng 92(6):551–570
68. Schmidt T, Balzani D (2015) Relaxed incremental variational approach for the modeling of damage-induced stress hysteresis in arterial walls. J Mechan Behav Biomed Mater 58:149–162
69. Ogden RW, Roxburgh DG (1999) A pseudo–elastic model for the Mullins effect in filled rubber. In Proceedings of the Royal Society of London A: Mathematical, Physical and Engineering Sciences (vol 455, No. 1988, pp. 2861-2877)
70. Dorfmann A, Ogden RW (2003) A pseudo-elastic model for loading, partial unloading and reloading of particle-reinforced rubber. Int J Solids Struct 40(11):2699–2714
71. Dorfmann A, Ogden RW (2004) A constitutive model for the Mullins effect with permanent set in particle-reinforced rubber. Int J Solids Struct 41(7):1855–1878
72. Dorfmann A, Pancheri FQ (2012) A constitutive model for the Mullins effect with changes in material symmetry. Int J Non-Linear Mech 47(8):874–887
73. Dorfmann A, Trimmer BA, Woods WA (2007) A constitutive model for muscle properties in a soft-bodied arthropod. J R Soc Interface 4(13):257–269
74. Naumann C, Ihlemann J (2015) On the thermodynamics of pseudo-elastic material models which reproduce the Mullins effect. Int J Solids Struct 69:360–369
75. Gracia LA, Peña E, Royo JM, Pelegay JL, Calvo B (2009) A comparison between pseudo-elastic and damage models for modelling the Mullins effect in industrial rubber components. Mechan Res Commun 36(7):769–776
76. Twizell EH, Ogden RW (1983) Non-linear optimization of the material constants in Ogden's stress-deformation function for incompressible isotropic elastic materials. The Journal of the Australian Mathematical Society. Series B. Appl Math 24(04):424–434
77. Latorre M, Montáns FJ (2014) What-You-Prescribe-Is-What-You-Get orthotropic hyperelasticity. Comput Mech 53(6):1279–1298
78. Sussman T, Bathe KJ (2009) A model of incompressible isotropic hyperelastic material behavior using spline interpolations of tension-compression test data. Commun Numer Methods Eng 25(1):53–63
79. Latorre M, Montáns FJ (2013) Extension of the Sussman-Bathe spline-based hyperelastic model to incompressible transversely isotropic materials. Comput Struct 122:13–26
80. Crespo J, Latorre M, Montáns FJ (2017) WYPIWYG hyperelasticity for isotropic, compressible materials. Comput Mechan 59:73–93
81. Latorre M, Montáns FJ (2017) WYPiWYG hyperelasticity without inversion formula: application to passive ventricular myocardium. Comput Struct 185:47–58
82. Latorre M, Peña E, Montáns FJ (2017) Determination and finite element validation of the WYPIWYG strain energy of superficial fascia from experimental data. Ann Biomed Eng 45(3):799–810
83. Romero X, Latorre M, Montáns FJ (2017) Determination of the WYPiWYG strain energy density of skin through finite element analysis of the experiments on circular specimens. Finite Elem Anal Des 134:1–15

84. Latorre M, Montáns FJ (2016) Fully anisotropic finite strain viscoelasticity based on a reverse multiplicative decomposition and logarithmic strains. Comput Struct 163:56–70
85. Latorre M, Montáns FJ (2015) Anisotropic finite strain viscoelasticity based on the Sidoroff multiplicative decomposition and logarithmic strains. Comput Mechan 56(3):503–531
86. Miñano M, Montáns FJ (2015) A new approach to modeling isotropic damage for Mullins effect in hyperelastic materials. Int J Solids Struct 67:272–282
87. Latorre M, Montáns FJ (2014) What-You-Prescribe-Is-What-You-Get orthotropic hyperelasticity. Comput Mechan 53(6):1279–1298
88. Bathe KJ (2014) Finite element procedures, 2nd edn. Watertown, KJ Bathe
89. Rausch MK, Humphrey JD (2015) A microstructurally inspired damage model for early venous thrombus. J Mechan Behav Biomed Mater 55:12–20
90. Gurtin ME, Francis EC (1981) Simple rate-independent model for damage. J Spacecraft Rockets 18(3):285–286
91. Neff P, Eidel B, Martin RJ (2016) Geometry of logarithmic strain measures in solid mechanics. Arch Ration Mechan Anal 222(2):507–572
92. Fiala Z (2016) Geometry of finite deformations and time-incremental analysis. Int J Non-Linear Mechan 81:230–244
93. Kearsley EA, Zapas LJ (1980) Some methods of measurement of an elastic strain-energy function of the Valanis–Landel type. J Rheol 24(4):483–500
94. Latorre M, Montáns FJ (2016) Stress and strain mapping tensors and general work-conjugacy in large strain continuum mechanics. Appl Math Model 40(5):3938–3950
95. Hayhurst D, Leckie FA (1973) The effect of creep constitutive and damage relationships upon the rupture time of a solid circular torsion bar. J Mechan Phys Solids 21(6):431–432
96. Murakami S, Ohno N (1981) A continuum theory of creep and creep damage. In Creep in structures, Springer, Heidelberg, pp 422–444
97. Ortiz M (1985) A constitutive theory for the inelastic behavior of concrete. Mechan Mater 4(1):67–93
98. Simo JC, Ju JW (1987) Strain- and stress-based continuum damage models-I. Formulation. Int J Solids Struct 23(7):821–840